

PREPARATION OF SILICA NANOPARTICLES IN REVERSED MICELLAR
SYSYTEMS

by

Ayşegül Dağlı

B.S., Chemistry, Boğaziçi University, 2006

Submitted to the Institute for Graduate Studies in
Science and Engineering in partial fulfillment of
the requirements for the degree of
Master of Science

Graduate Program in Chemistry
Boğaziçi University
2009

To my family...

ACKNOWLEDGEMENTS

First and foremost, I would like to deeply thank my supervisor Prof. Dr. N. Zeynep Atay for her invaluable understanding as well as her encouragement made it possible to complete this study. Especially I want to thank her for being with me when I have difficulties in my personal life.

I would like to thank my committee members Prof. Orhan Yenigün and Assis. Prof. Amitav Sanyal for giving their valuable time for reviewing the final manuscript and for their constructive comments and suggestions.

I thank my lab mate, Melis Çağdaş, firstly for her friendship and for being with me anytime I need. I also thank her for her suggestions and help during the project.

I would like to also thank to the research student Ezgi Kılıç for her help and luck.

I am grateful to Dr. Sinan Şen for his cooperation in never-ending particle size analysis, to Dr. Bilge Gedik for SEM analysis and to Dr. Ceyda Uyguner for the fluorescence measurements. I would like to extend my thanks to all members of the Chemistry Department and to our kind secretary, Hülya Metiner for their help.

I also thank the Sanyal group, especially Idil Ipek Yılmaz, for the Bodipy dye and. I need also thank them, Prof. Duygu Avcı and her students for the nitrogen we used during this study.

I am really grateful to my friends Sevgi Şenel, Gamze Şen, Onur Özdiñ and especially to Bahar Yeniad for their accompany and encouragement.

Last and surely not least, I thank all my family, especially my sisters and mom.

Financial support of this work was provided by Boğaziçi University Research Fund (Project Number: 08B502)

ABSTRACT

PREPARATION OF SILICA NANOPARTICLES IN REVERSED MICELLAR SYSTEMS

When surfactants are in apolar media, they form reverse micelles by encapsulating a water droplet inside their hydrophilic head groups. The hydrophilic core of the water droplet which is dispersed in the oily apolar environment can solubilize water-soluble species and can be used as a microreactor for a number of reactions. The aim of this study is to use these hydrophilic cores of reverse micelles as a microreactor to synthesize fluorescent dye-doped silica nanoparticles.

Both anionic and nonionic surfactants have been used to prepare reverse micelles. Silica nanoparticles were prepared inside the droplet cores and the effects of changing the surfactant, as well as the size of the dispersed droplets, on the particle size were investigated. Since the fluorescence dye-doped silica nanoparticles can be used as labeling agents for biomolecules, these nanoparticles were then doped with three different types of fluorescent dyes while forming inside the dispersed droplets and their optical properties were investigated.

It has been observed that the silica nanoparticle size can be controlled by changing the water-to-surfactant molar ratio, i.e. the droplet size. The fluorescent emission spectrum results have shown that the doping with inorganic hydrophilic dye Ru(bipy)₃ was highly successful. When the dye was changed to amphiphilic Rhodamine 101 and more hydrophobic Bodipy, structural dye-modification seemed to be necessary to achieve doping.

ÖZET

TERSİNİR MİSELLERDE SİLİS NANOPARÇACIKLARININ HAZIRLANMASI

Yüzey-aktif maddeler apolar ortamda iken hidrofilik baş grupları ile su damlacıklarını hapsederek tersinir miseller oluştururlar. Apolar yağlı ortamda dağılmış su damlacıklarının hidrofilik çekirdeğinde, suda çözünür pek çok madde çözündürülebilir ve bu çekirdek birçok tepkime için mikro reaktör görevi görebilir. Bu çalışmanın amacı tersinir misellerin hidrofilik çekirdeklerini floresan boya ile doldurulmuş silis nanoparçacıklarının sentezlenmesinde mikroreaktör olarak kullanmaktır.

Tersinir miselleri kararlı kılmak için hem anyonik hem de iyonik olmayan yüzey-aktif maddeler kullanılmıştır. Silis nanoparçacıklar su damlacıkları içinde sentezlenmiş, ve yüzey-aktif madde değişimi ile damlacık boyutunun parçacık boyutu üzerindeki etkileri çalışılmıştır. Flurosan boyar madde ile doldurulan silis nanoparçacıklarının biyomoleküllerin işaretlemeye kullanım alanları olması nedeniyle, bu nanoparçacıklar su damlacıkları içinde oluşurken, üç farklı flurosan boyar madde ile doldurulmuş ve optik özellikleri incelenmiştir.

Silis nanoparçacıklarının boyutunun su-yüzey-aktif madde molar oranına, yani damlacık boyutuna, bağlı olarak değiştirilebileceği görülmüştür. Parçacıkların floresan emisyon spektrumu incelendiğinde anorganik Ru(bipy)₃ boyar madde ile doldurma işleminin başarılı olduğu görülmüştür. Boyar madde anfililik Rhodamine 101 ve daha hidrofobik Bodipy olarak değiştirildiğinde, doldurulma işleminin oluşabilmesi için boyar maddede yapısal değişiklikler gerektiği saptanmıştır.

TABLE OF CONTENTS

ACKNOWLEDGEMENTS	IV
ABSTRACT	V
ÖZET	VI
LIST OF FIGURES	X
LIST OF TABLES	XIV
LIST OF SYMBOLS/ABBREVIATIONS	XV
1. INTRODUCTION	1
1.1. General	1
1.2. Silica Nanoparticles	2
1.2.1. General	2
1.2.2. Methods for Synthesis of Silica NPs	5
1.2.3. Reversed Micellar Systems	6
1.2.3.1. Surfactants	6
1.2.3.2. Self-Assembly and Packing Ratio	8
1.2.3.3. Droplet Size	11
1.2.4. The Mechanism of Particle Formation	14
1.2.5. Techniques in NP characterization	18
2. REAGENTS AND INSTRUMENTS	21
2.1. Reagents	21
2.1.1. Surfactants and Cosurfactants	21
2.1.1.1 . Sodium dioctylsulfosuccinate (AOT)	21
2.1.1.2 . Triton X-100	21
2.1.1.3 . N-Hexanol	21
2.1.2. Nonpolar Solvents	21
2.1.2.1 . Cyclohexane	21
2.1.2.2 . N-Decane	21
2.1.2.3 . N-Heptane	21
2.1.3. Ammonia solution	22
2.1.4. Deionized water	22
2.1.5. Absolute ethanol	22

2.1.6. Fluorescent Dyes	22
2.1.6.1 . Rhodamine 101.....	22
2.1.6.2. Tris (2'2-bipyridine)ruthenium(II) chloride hexahydrate	23
2.1.6.3. Bodipy	23
2.1.7. Tetraethyl orthosilicate (TEOS)	24
2.2. Instruments	25
2.2.1. Analytic Balance	25
2.2.2. Centrifuge	25
2.2.3. Sonicator.....	25
2.2.4. Oven	25
2.2.5. UV-VIS Spectrophotometer	25
2.2.6. Fluorescence Spectrophotometer	25
2.2.7. Particle Size Analyzer	26
2.2.8. Scanning Electron Microscope.....	26
2.2.9. Fourier Transform Infrared (FTIR) Spectrophotometer.....	26
3. EXPERIMENTAL METHODS	27
3.1. Preparation of AOT Stock Solution	27
3.2. Preparation of Dye Solutions	27
3.3. Preparation Procedure of Silica NPs in Reversed Micelles	27
3.3.1. AOT-stabilized Reversed Micelles	27
3.3.2. Triton X-100-stabilized Reversed Micelles	28
3.4. Scheme of the Reaction.....	28
3.5. IR Measurements.....	29
3.6. Particle Size Measurements.....	29
3.7. SEM Measurements	30
3.8. UV/VIS Measurements	30
3.9. Fluorescence Measurements.....	30
4. RESULTS AND DISCUSSIONS	32
4.1. General Remarks and Visual Observations.....	32
4.3. Particle Size Results	34
4.4 UV/VIS and Fluorescence Results	39
5. CONCLUSION	46
6. SUGGESTIONS FOR FUTURE WORK	47

APPENDIX A: THE PARTICLE SIZE ANALYZER RESULTS.....	48
APPENDIX B: SEM RESULTS.....	65
REFERENCES.....	72

LIST OF FIGURES

Figure 1. 1. Fluorescent signal amplification using dye-doped nanoparticles a) pure water b) tetramethyl rhodamine dye (TMR) c) TMR doped silica nanoparticles	3
Figure 1. 2. Schematic representation of surface modification of silica NPs	4
Figure 1. 3. Schematic representation of detection of DNA with silica NP	5
Figure 1. 4. Schematic representation of a surfactant molecule	6
Figure 1. 5. The structure of the anionic surfactant, sodium dioctylsulfosuccinate	7
Figure 1. 6. An example for a zwitterionic surfactant, Cocaamidopropyl betaine	7
Figure 1. 7. The structure of the cationic surfactant, cetyltrimethylammonium	7
Figure 1. 8. The structure of the nonionic surfactant, Polyethylene glycol.....	7
Figure 1. 9. Scheme for the critical micelle concentration (CMC).....	8
Figure 1. 10. Formation of the micelle	8
Figure 1. 11. Formation of the reversed micelle.....	9
Figure 1. 12. Schematic representation of a surfactant (AOT) molecule showing the.....	10
Figure 1. 13. The effect of the water content on the droplet size	11
Figure 1. 14. The effect of water-to-surfactant molar ratio R on particle size by using...	13
Figure 1. 15. The effect of water to surfactant molar ratio R on particle size by using a nonionic surfactant	14
Figure 1. 16. Reaction scheme for TEOS hydrolysis a) Base-catalyzed hydrolysis of....	16
Figure 1. 17. Growth mechanism of silica NPs in the reversed micellar system	16
Figure 1. 18. Mechanism for formation of dye-doped silica NPs in reversed micellar systems.....	17

Figure 1. 19. Typical TEM images showing the particle growth during the TEOS hydrolysis in reversed micelles	19
Figure 1. 20. Typical SEM image of particles produced by the Stöber method.....	20
Figure 2. 1. The structure of Rhodamine 101 dye.....	22
Figure 2. 2. The structure of Ru(bipy) ₃ dye	23
Figure 2. 3. The structure of Bodipy dye.....	24
Figure 2. 4. The structure of TEOS	24
Figure 3. 1. Reaction Scheme.....	29
Figure 4. 1. The IR spectra of solid silica NPs recovered from AOT-stabilized reversed micelles.....	33
Figure 4. 2. The IR spectra of amorphous silica [30]	33
Figure 4. 3. Absorbance versus wavelength plot of Ru(bipy) ₃ in water.....	39
Figure 4. 4. Absorbance versus wavelength plot of sample S10 (blue) and S11 (pink) in aqueous media.....	40
Figure 4. 5. Absorbance versus wavelength plot of sample S12 in aqueous media	40
Figure 4. 6. Fluorescence emission spectra of pure Ru(bipy) ₃ (blue), sample S11 (pink), S10 (yellow) and S9 (green) in aqueous media	41
Figure 4. 7. Fluorescence emission spectra of sample S12 in aqueous media	42
Figure 4. 8. Absorbance versus wavelength plot of pure Rhodamine 101 dye in aqueous media.....	43
Figure 4. 9. Absorbance versus wavelength plot of pure bodipy dye in NH ₃ (aq)	44
Figure A. 1. Particle size data of sample S1.....	49
Figure A. 2. Particle size data of sample 040308-5	50
Figure A. 3. Particle size data of sample S3	51
Figure A. 4. Particle size data of sample S4	52

Figure A. 5. Particle size data of sample S5	53
Figure A. 6. Particle size data of sample S6	54
Figure A. 7. Particle size data of sample S7	55
Figure A. 8. Particle size data of sample S8	56
Figure A. 9. Particle size data of sample S10	57
Figure A. 10. Particle size data of sample S11	58
Figure A. 11. Particle size data of sample S13	59
Figure A. 12. Particle size data of sample S14	60
Figure A. 13. Particle size of sample S15.....	61
Figure A. 14. Particle size data of sample S16	62
Figure A. 15. Particle size data of sample S10 in water (sonicated 5hours)	63
Figure A. 16. Particle size data of sample S10 in water (after 25hours)	63
Figure A. 17. Particle size data of sample S14 in water (after 25hours)	64
Figure A. 18. Particle size data of sample S14 in water (after 5days).....	64
Figure B. 1. SEM image of sample S1.....	65
Figure B. 2. SEM image of sample S3	66
Figure B. 3. SEM image of sample S4	66
Figure B. 4. SEM image of sample S10	67
Figure B. 5. SEM image of sample S8	67
Figure B. 6. SEM image of sample S9	68
Figure B. 7. SEM image of sample S10	68
Figure B. 8. SEM image of sample S11	69
Figure B. 9. SEM image of sample S12	69
Figure B. 10. SEM image of sample S13	70
Figure B. 11. SEM image of sample S14	70

Figure B. 12. SEM image of sample S15 71

Figure B. 13. SEM image of sample S16 71

LIST OF TABLES

Table 1. 1. Structures formed by different packing ratios	10
Table 4. 1. List of samples.....	34
Table 4. 2. Particle size values compared with the values in literature	35
Table 4. 3. Particle size values for empty and doped NPs.....	36
Table 4. 4. Particle Size Comparison.....	37
Table 4. 5. Minimum and maximum particle size values measured with SEM	38
Table 4. 6. Particle size values in aqueous media.....	38

LIST OF SYMBOLS/ABBREVIATIONS

a_0	Surfactant head group area
h	water-to-TEOS molar ratio
l	Optimum length of the surfactant tail
r_{core}	Core radius of the droplets
r_h	Hydrodynamic radius of the droplets
R	water-to-surfactant molar ratio
P	Packing ratio
V	Volume of the surfactant
V_m	Molar Volume
AOT	Sodium dioctylsulfosuccinate
Bodipy	Boron dipyrromethene
CTAB	Cetyltrimethylammonium bromide
FTIR	Fourier Transform Infra Red Spectroscopy
IR	Infra Red
NP	Nanoparticle
SEM	Scanning Electron Microscopy
TEOS	Tetraethyl orthosilicate
TMR	Tetramethyl rhodamine
TEM	Transmission Electron Microscopy
UV/VIS	Ultra Violet Visible Spectroscop

1. INTRODUCTION

1.1. General

In therapeutic applications it is very important to identify and characterize the intracellular events. The invisible biomolecules can be labeled with a fluorescent compound to study these interactions. Mostly organic fluorophores, which have high quantum yield, are used as labeling reagents; however they have limited sensitivity and photostability [1].

As an alternative to the organic fluorophores several nanomaterials are currently being used as labeling reagents. These nanomaterials include metallic nanoparticles (NPs), quantum dots (QDs), magnetic NPs, and silica NPs.

The most common metallic NP in the literature is gold (Au) NP. These Au-NPs are also known as colloidal gold, are suspension of Au particles in a solvent, usually water. Conjugates of Au NPs and oligonucleotides are of great interest as biomarkers in the analysis of a number of biomolecules such as proteins and carbohydrates [2].

Another alternative to the organic fluorophores are QDs. QDs are semiconductor crystals (eg. CdSe, CdTe, CdS, ZnSe, PbS) which provide bright fluorescence and they are also more photostable compared to the organic fluorophores. However, these QDs remain photostable only in apolar media [3].

Magnetic NPs can also be used instead of organic fluorophores. Because of their superparamagnetism, magnetic NPs, most commonly iron NPs (Fe NPs), have different application areas in biomedicine and biotechnology such as cell labeling and separation, magnetic resonance imaging contrast reagent [4].

Generally, NPs have unique optical properties, high surface-to-volume ratio and other size dependent qualities. When these qualities are combined with surface modifications, they can provide highly sensitive and selective bioassays [5].

The aim of this study is to synthesize fluorescent dye doped silica NPs in the core of the dispersed water droplets of reversed micelles. Both anionic and nonionic surfactants have been used in the formation of the reversed micelles. Doping has been done with various fluorescent dyes and the NPs are characterized. A brief introduction to silica NPs is given below.

1.2. Silica Nanoparticles

1.2.1. General

Silica NPs are widely used in many bioanalysis applications. They are used in labeling by incorporating a fluorescent dye into the silica matrix. As the silica matrix serves as a barrier to the environment, both photobleaching and photodegradation can be minimized [1]. Moreover, dye-doped silica NPs produce highly amplified optical signal compared with a single dye molecule since a large number of dye molecules can be incorporated into the silica matrix [5].

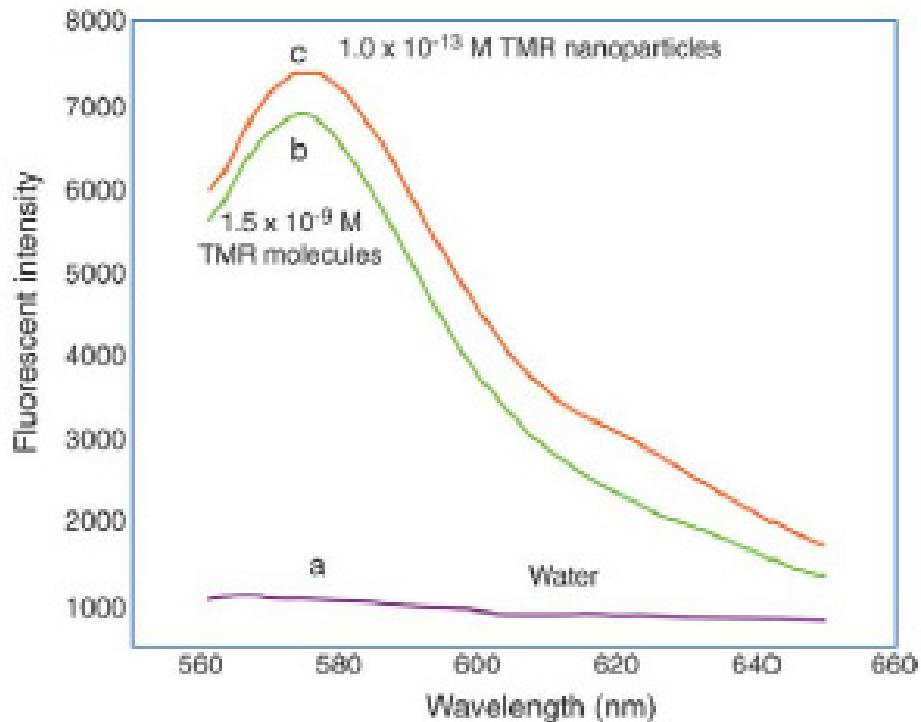


Figure 1. 1. Fluorescent signal amplification using dye-doped nanoparticles a) pure water b) tetramethyl rhodamine dye (TMR) c) TMR doped silica nanoparticles [5]

Polymer-based NPs have also been used in bioanalysis and labeling. However silica NPs are preferred over the polymer-based NPs because they show less aggregation and little dye leakage [6].

The high sensitivity of the fluorescence signal enhancement and selectivity can be inhibited by the irreversibly accumulation of silica NPs and cause non-specific binding. The particles can bind to various chemical and biological species, which can lead to false signal. To prevent the unspecific binding, different functional groups can be attached onto the silica surface for conjugation with the desired biomolecules [7]. The surface of the silica NPs can be functionalized by additional coating with various alkoxy silanes, such as carboxyethylsilanetriol for introduction of carboxylic acid groups (-COOH), 3-aminopropyltriethoxysilane for amino groups (-NH₂), or 3-mercaptopropyl trimethoxysilane for thiol groups [7, 8].

In Figure 1.2 some surface modifications of the silica NPs are shown. In this figure an alternative approach for surface modification based on ionic interaction is also shown.

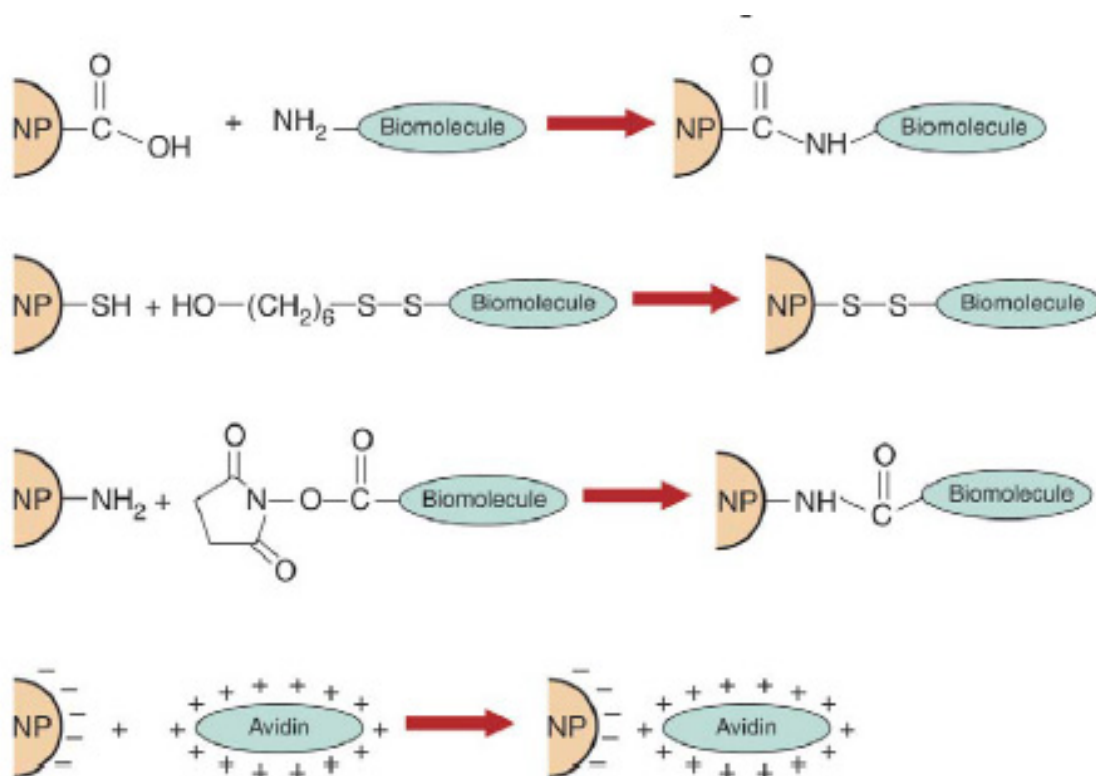


Figure 1. 2. Schematic representation of surface modification of silica NPs [9]

All these qualities make silica NPs excellent labeling reagents in bioanalysis.

In the literature, there are many examples for the applications of the silica NPs. They are used in DNA detection [10]. As shown in Figure 1.3 DNA 1 is captured on to the glass surface. Then DNA 2 is added for hybridization. In the last step probe DNA (DNA 3), which is labeled with dye-doped silica NP, is added. After several washing steps, DNA 2 is detected by monitoring the fluorescence signals of the probe DNA. The conjugation of the probe DNA with the silica NP is carried out by modifying the surface of the silica NP with positively charged avidin layer [10].

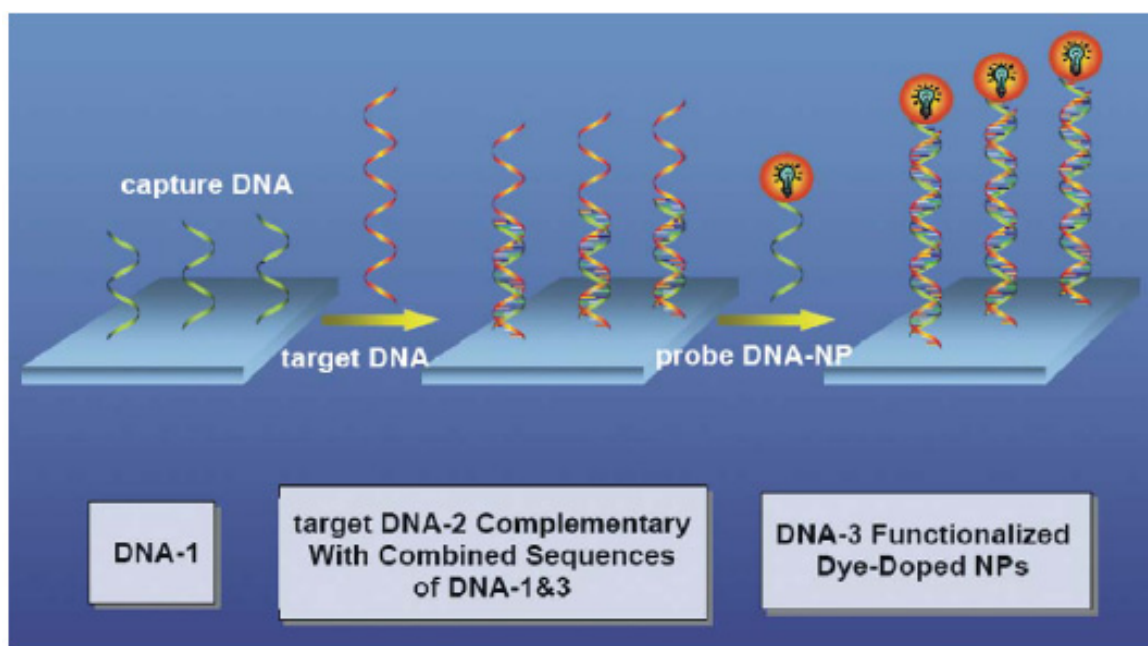


Figure 1. 3. Schematic representation of detection of DNA with silica NP [10]

Silica NPs has also been used in clinical diagnostic applications. Two-particle assay, which is composed of one dye-silica NP and the other particle with a magnetic core for magnetic collection, was able to collect leukemia cells from a spiked blood sample [11, 12].

The surface of the silica NPs can be modified with various antibodies; hence the NP can bind to the corresponding antigen and recognize the molecule [13, 14].

1.2.2. Methods for Synthesis of Silica NPs

There are two general methods used in the synthesis of silica based NPs: a) synthesis in the reversed micelles [15-17], and b) Stöber method [18].

The widely used Stöber method is a one step reaction, involving condensation of tetraethyl orthosilicate (TEOS) in bulk ethanol: water mixtures under basic conditions [18]. Both organic and inorganic dyes can be incorporated into the silica matrix using this method [19]. However, because of the hydrolysis procedure, the NPs have a large size distribution [13]. So, this method requires further filtration steps.

The second, reversed micellar method is based on the formation of water-in-oil (w/o) microemulsion. It requires the use of surface-active-agent (surfactant) and oil, and involves condensation of the TEOS in the water core of the microemulsion. Mostly inorganic dyes can be incorporated into the silica matrix using this method. The particle size can be controlled by changing the nature of the surfactant and the water-to-surfactant ratio.

1.2.3. Reversed Micellar Systems

1.2.3.1. Surfactants. Surfactants also known as emulsifiers, detergents, wetting agents, are amphiphilic compounds which have a hydrophilic head group and a hydrophobic tail. Therefore they are soluble both in oil and water. They lower the interfacial tension between two immiscible liquids.

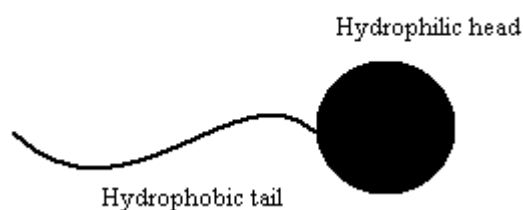


Figure 1. 4. Schematic representation of a surfactant molecule

Surfactants are classified as anionic, cationic, non-ionic or zwitterionic according to change of their head groups.

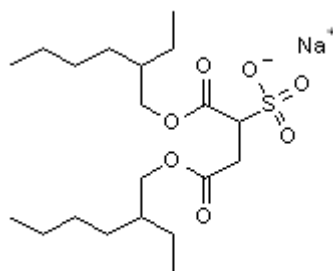


Figure 1. 5. The structure of the anionic surfactant, sodium dioctylsulfosuccinate (AOT)

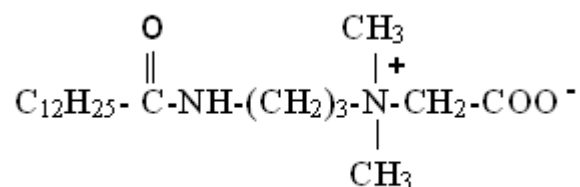


Figure 1. 6. An example for a zwitterionic surfactant, Cocaamidopropyl betaine

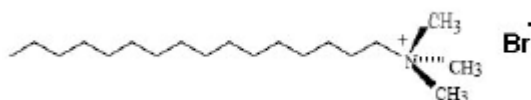


Figure 1. 7. The structure of the cationic surfactant, cetyltrimethylammonium bromide, (CTAB)

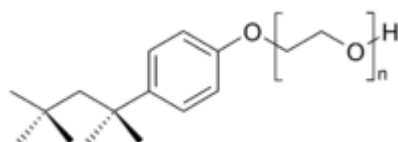


Figure 1. 8. The structure of the nonionic surfactant, Polyethylene glycol p-(1,1,3,3 Tetramethylbutyl)-phenyl ether, (Triton X-100)

1.2.3.2. Self-Assembly and Packing Ratio. As being amphiphilic, surfactants can assemble in the bulk solution into variety of aggregate structures.

The simplest aggregate structure is called a micelle. Micelles can only form at a certain surfactant concentration which is the critical micelle concentration (CMC).

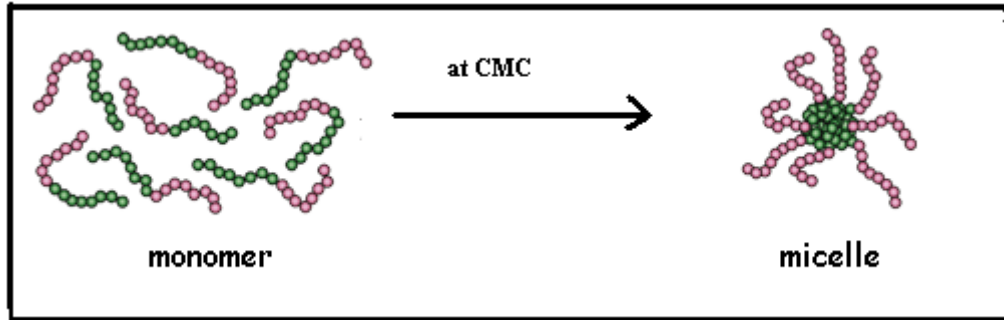


Figure 1. 9. Scheme for the critical micelle concentration (CMC)

When micelles form in water, the hydrophobic tails of surfactants form a core of oily (i.e. hydrophobic) nature and the hydrophilic head groups of the surfactants are in contact with water.

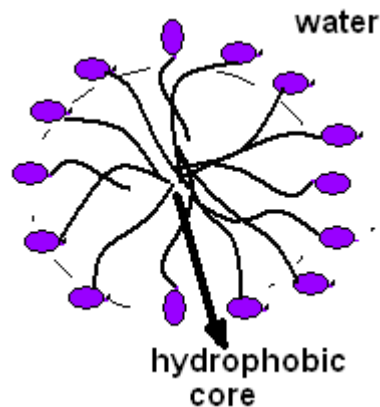


Figure 1. 10. Formation of the micelle

When surfactants are in oil-continuous medium, they form reverse micelles where the hydrophilic head groups form a core encapsulating a water droplet inside and the hydrophobic tails are in contact with the oil phase.

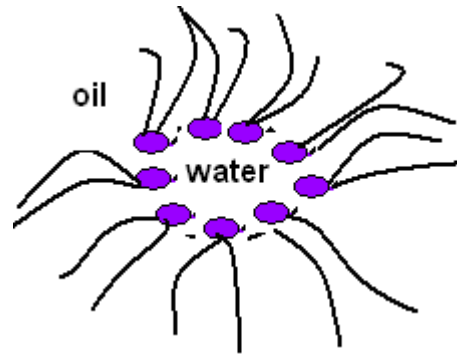


Figure 1. 11. Formation of the reversed micelle

Formation of micelles or reversed micelles depends on the packing of the surfactants in an aggregate, i.e. the packing ratio, P .

$$P = \frac{V}{a_0 \times l} \quad (1.1)$$

Where V is the volume of the surfactant tail, l is the optimum length of the surfactant tail and a_0 is the area of the surfactant head group.

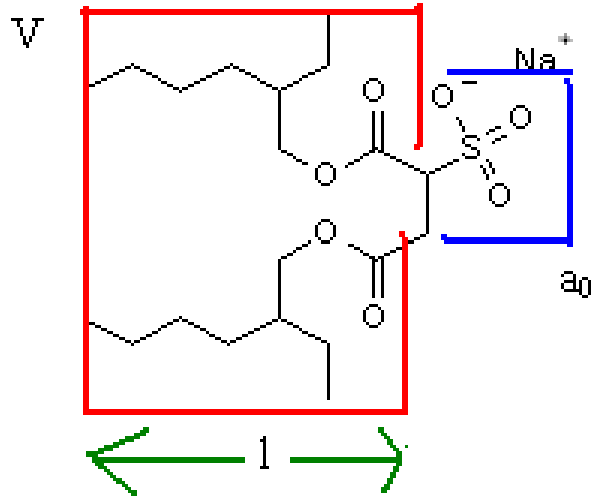


Figure 1. 12. Schematic representation of a surfactant (AOT) molecule showing the parameters in the packing ratio

Shape of the surfactant aggregates formed is determined by their P . These are summarized in Table 1.1.

Table 1. 1. Structures formed by different packing ratios [20]

P	< 1/3	1/3-1/2	1/2-1	1	>1
Structure	Spherical micelles	Cylindrical micelles	Vesicles	Planer bilayers	Reverse micelles
					

If the packing ratio of the surfactant is greater than 1, then reversed micelles (also known as water-in-oil (w/o) microemulsion) are formed. The core of the w/o microemulsions are polar microenvironments, which can be utilized for a number of chemical reactions including the preparation of some colloidal particles.

In this work, the polar core of reversed micelles has been used as a microreactor for the synthesis of the silica NPs.

1.2.3.3. Droplet Size. In micellar systems and reversed micellar systems the droplet size can be controlled. When more oil is added to the micellar systems or more water is added to the reversed micellar systems the droplet size becomes greater.

The size of oil droplets increase by addition of oil to the n-micelles in water. Similarly, upon addition of water to reversed micellar systems, the size of the dispersed H₂O droplets gets enlarged.

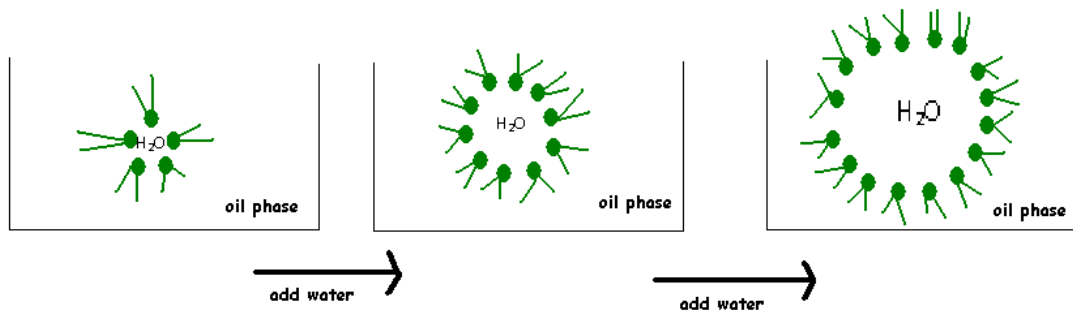


Figure 1. 13. The effect of the water content on the droplet size

The droplet size of the reversed micelles can be controlled by changing the water content. The core radius of the droplets can be calculated by the following formula:

$$r_{core}/nm = \frac{3V_m}{a_0} \frac{[H_2O]}{[surfactant]} = \frac{3V_m}{a_0} R \quad (1.2)$$

$$\text{where } R = \frac{[H_2O]}{[surfactant]}$$

The first term in the formula $\left(\frac{3V_m}{a_0}\right)$ is a known value for surfactants. The second term in the formula $\left(\frac{[H_2O]}{[\text{surfactant}]}\right)$ can be changed to obtain the desired radius for the droplets. The ratio $\left(\frac{[H_2O]}{[\text{surfactant}]}\right)$ is called the R value. For example $\left(\frac{3V_m}{a_0}\right)$ value for the anionic surfactant, sodium dioctyl sulfosuccinate (AOT), has been determined to be 0.175 nm [21]. Hence the core and hydrodynamic radius, which is the radius including the length of the surfactant tail, of the droplets of AOT-stabilized reversed micelles can be calculated using the following formulas:

$$r_{core}/nm = 0.175R \quad (1.3)$$

$$r_h/nm = 0.175R + 1.5 \quad (1.4)$$

where 1.5 nm is the length of the surfactants tail.

This way, the reaction environment and so the solid particle size can be controlled if the silica NPs are to be synthesized in the core of the w/o microemulsions.

Osseo-Assare and Arrigada [15, 22-25] have synthesized silica NPs in AOT-stabilized reversed micelles and in nonionic surfactant-stabilized reversed micelles, where the surfactant was polyoxyethylene (5) nonlyphenylether, shortly NP-5. They investigated the growth kinetics and effects of the water/surfactant molar ratio and ammonia concentration on the particle growth. They found that the particle size increases by the addition of ammonia which is used as a catalyst in the reaction. As seen in Figure 1.14, particle size increases as R increases in the range 5-9.5 when they use the anionic surfactant AOT. However as shown in Figure 1.15 the particle size has a minimum versus R when they used the nonionic surfactant NP-5.

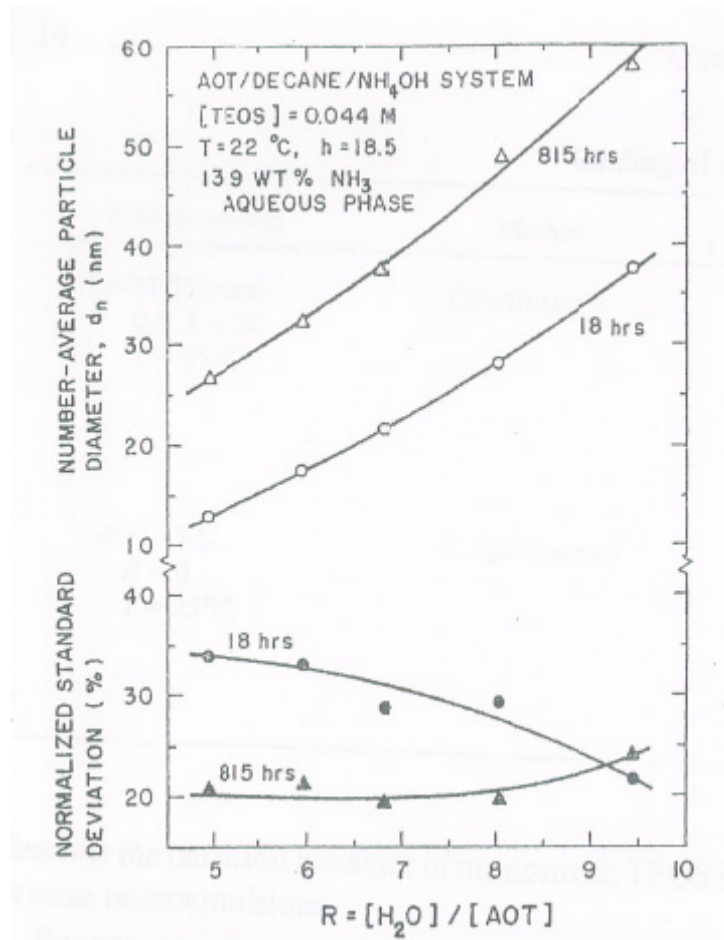


Figure 1. 14. The effect of water-to-surfactant molar ratio R on particle size by using an anionic surfactant [23]

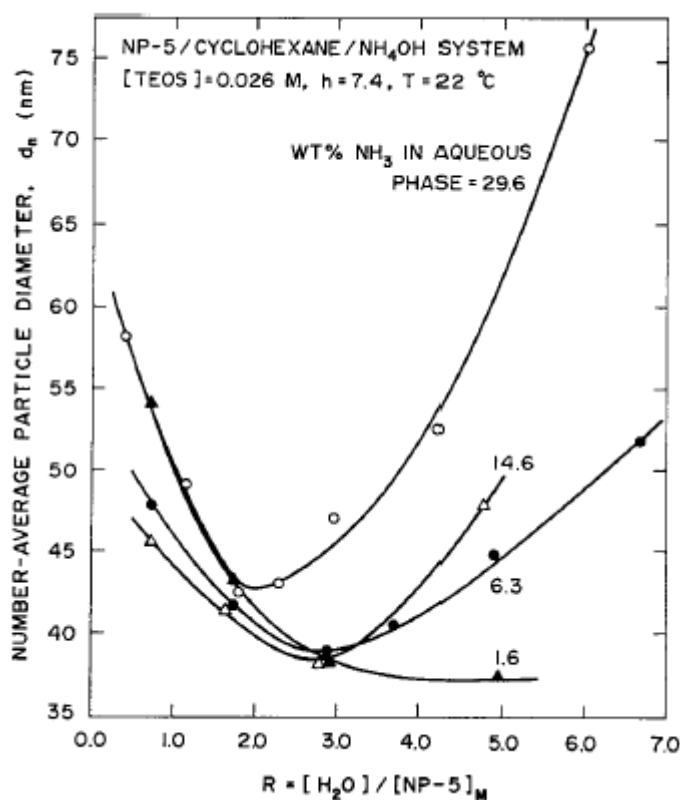


Figure 1. 15. The effect of water to surfactant molar ratio R on particle size by using a nonionic surfactant [24]

1.2.4. The Mechanism of Particle Formation

Preparation of silica NPs is based on the hydrolysis and polycondensation reactions of TEOS. As shown in Reaction 1.4, overall, TEOS reacts under basic conditions with water to produce silica (SiO₂) and alcohol. Usually ammonia is used as a base catalyst. It serves both as a catalyst and as a water source. Proposed mechanism is said follow one or more of the following routes shown in Reaction 1.1-1.4 [26].

In the hydrolysis step silanol groups (-Si-OH) are produced which can react with another silicate molecule to produce alcohol and to form Si-O-Si bond. Another possibility is that the produced silanol groups react with another silanol group to form water and Si-O-Si bond at the end.

Hydrolysis:



Alcohol Condensation:



Water Condensation:



Overall Reaction:



Growth of the particles depends on the hydrolysis rate of TEOS. In order to obtain particles with desired properties, hydrolysis of the TEOS should be controlled. Using reversed micelles as the synthesis method provides a controlled medium for the reaction by solubilizing both polar and nonpolar reagents in defined locations. [15]. As shown in Figure 1.16, when hydrolysis of TEOS take place in the reversed micelles, the aqueous core of reverse micelles provide a controlled medium. In Stöber method, hydrolysis of TEOS takes place in the bulk alcohol, which is not a controlled medium. However, in both methods, as shown in Figure 1.16.a, $\text{NH}_3(\text{aq})$ produces an OH^- group and this OH^- group attacks to the Si atom by kicking out one -OR group. It is a secondary nucleophilic substitution (S_N^2) type reaction.

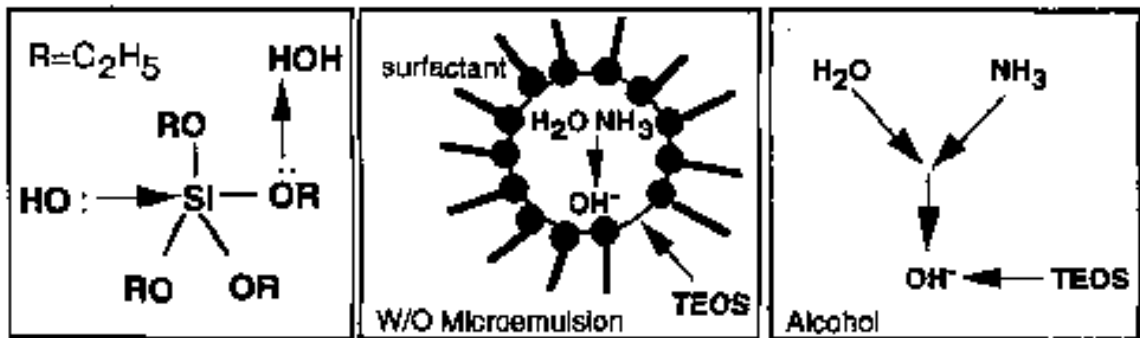


Figure 1. 16. Reaction scheme for TEOS hydrolysis a) Base-catalyzed hydrolysis of TEOS (left); b) Ammonia-catalyzed TEOS hydrolysis in reversed micelles (middle); c) in ethanol media (Stöber) (right) [26]

During the reaction in reverse micelles, TEOS can enter from oil phase into the aqueous phase, and can be hydrolyzed in the empty aqueous core of the reversed micelles, and then transferred to a particle-filled aqueous core of another reverse micelle, or unhydrolyzed TEOS can interact with a particle-filled reversed micelle in which hydrolysis of TEOS takes place in the water-shell or hydration layer (Figure 1.17) [22].

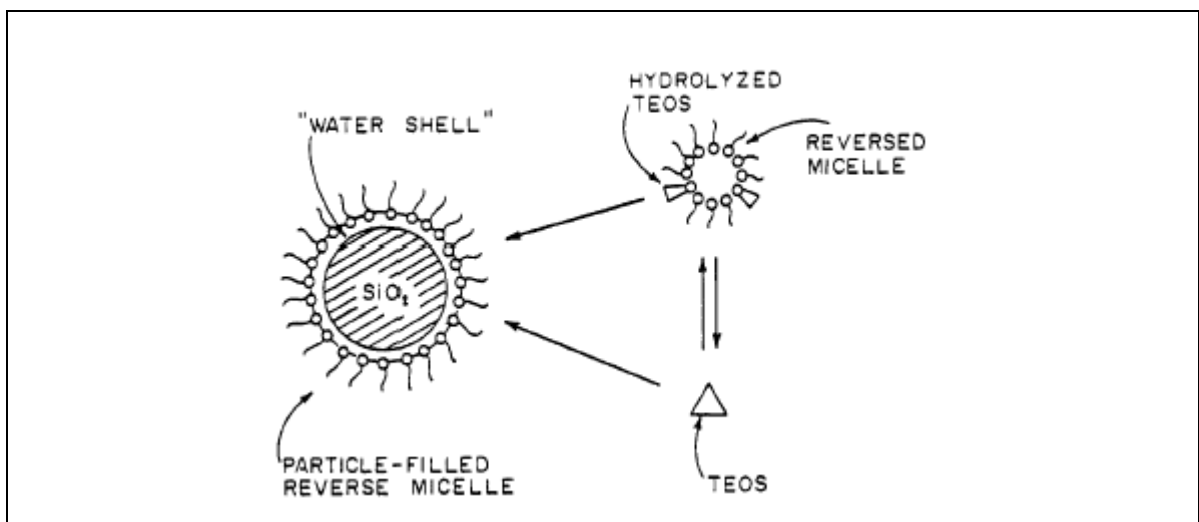


Figure 1. 17. Growth mechanism of silica NPs in the reversed micellar system [22]

Hydrolysis of TEOS in an empty reverse micelle is more significant than the hydrolysis in a particle-filled reverse micelle. The hydrolyzed TEOS in empty reverse micelle is the main source of monomer for particle growth.

In order to synthesize dye-doped silica nanoparticles, the dye must be hydrophilic so it goes to the polar core of the reverse micelles. When TEOS is added to the microemulsion it is hydrolyzed and forms the silica matrix by encapsulating the dye into it. To dope the silica with hydrophobic dyes, dyes must be modified with dextran initially to make them hydrophilic [6].

In Figure 1.18, it is shown how a hydrophilic dye, in this case Tris (2'-bipyridine)ruthenium(II) chloride hexahydrate; $\text{Ru}(\text{bpy})_3$, is doped into silica NPs. By addition of $\text{Si}(\text{OEt})_4$, TEOS, into the dye containing reversed micelles, both dye and TEOS go to the hydrophilic core of the reversed micelles. TEOS hydrolysis by producing silanol groups and the condensation reactions take place. During these condensation reactions silica matrix is built as shown in the first step and hydrophilic dye is encapsulated into the silica matrix as shown in the second step in Figure 1.18.

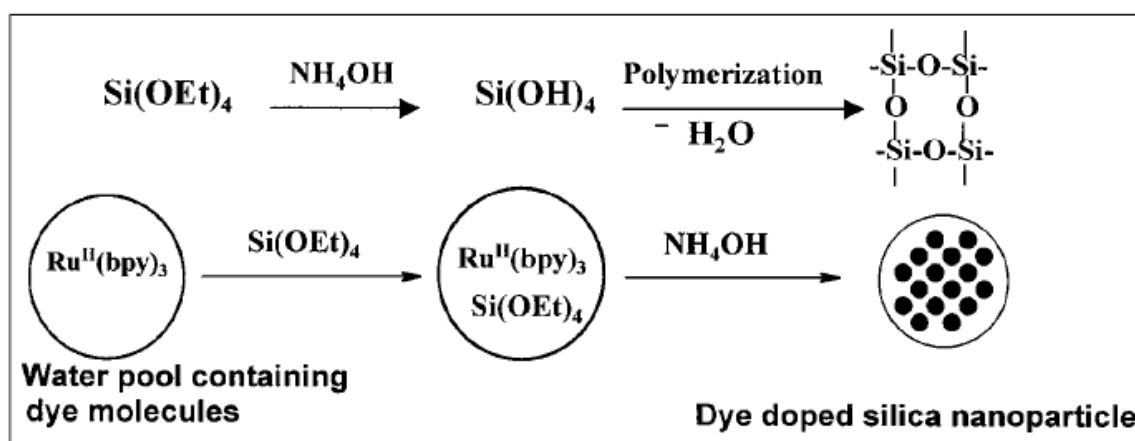


Figure 1. 18. Mechanism for formation of dye-doped silica NPs in reversed micellar systems [6]

1.2.5. Techniques in NP characterization

The dye-doped silica NPs are characterized for the particle size and optical properties since these features are important in deciding whether or not they can be used in bioanalysis. Transmission electron microscopy (TEM), scanning electron microscopy (SEM) or light scattering are the widely used methods for particle size determination [27].

TEM is a microscopic technique where a beam of electrons is transmitted through an ultra thin sample. As the electrons pass through the sample, they interact with it. An image formed from the electrons transmitted through the sample, is magnified and focused by an objective lens and appears on an imaging screen [28].

In most studies the particle size is investigated by TEM. Chang et al. have followed up the growth of the silica NPs by taking the TEM images of the particles at different reaction times (Figure 1.29) [26].

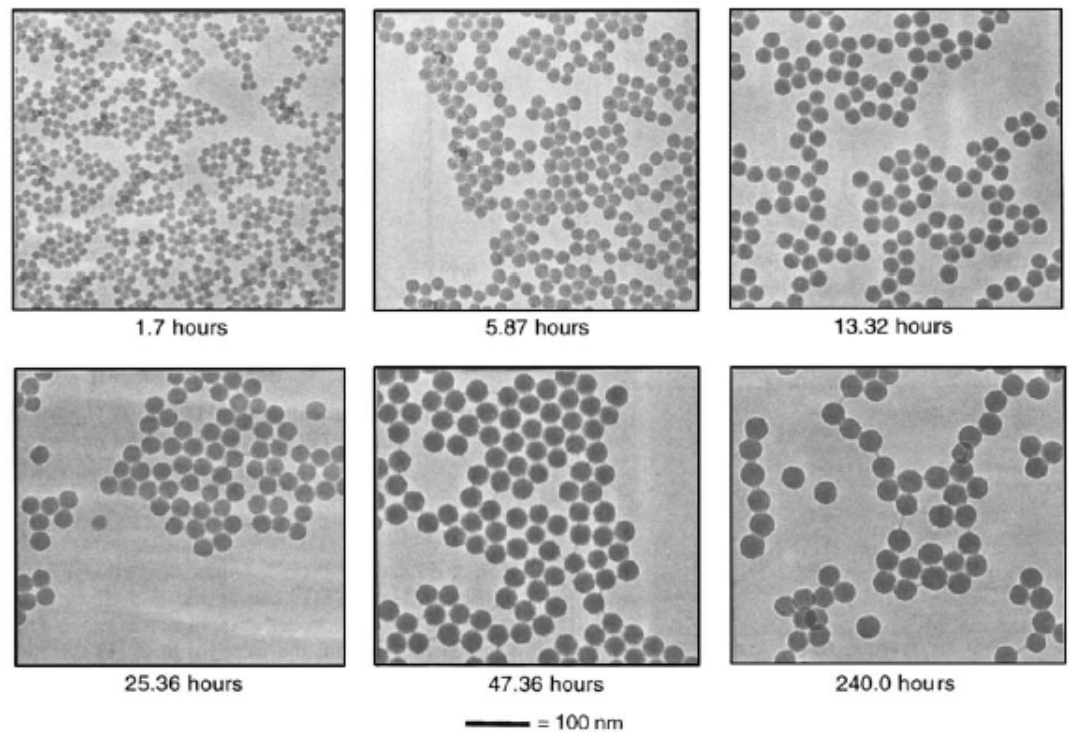


Figure 1. 19. Typical TEM images showing the particle growth during the TEOS hydrolysis in reversed micelles [26]

Another method for the particle size detection is SEM in which a sample surface is scanned with a beam of electrons. These electrons interact with the sample surface, producing an image of the surface. By analyzing this image, size of the particles can be determined.

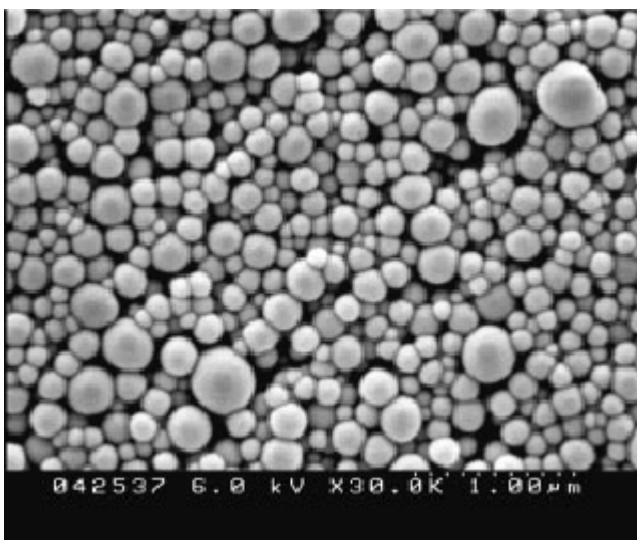


Figure 1. 20. Typical SEM image of particles produced by the Stöber method [6]

Optical properties of the particles can be investigated by the fluorescence spectroscopy and UV-VIS spectroscopy. The fluorescent intensities of solutions with pure dye in them and the solutions containing dye-doped silica NPs can be compared using this method (Figure 1.1). Photobleaching experiments, which show whether the dye remains photostable when doped into the silica matrix, can be also carried out by using these spectroscopic methods [6].

2. REAGENTS AND INSTRUMENTS

2.1. Reagents

2.1.1. Surfactants and Cosurfactants

2.1.1.1. Sodium dioctylsulfosuccinate (AOT) The double chained anionic surfactant, obtained from Sigma Chemicals, was used to form reversed micelles. It was used without further purification.

2.1.1.2. Triton X-100 Nonionic Triton X-100 was obtained from Merck. It is in liquid form and was used without further purification. It was also used to form reversed micelles.

2.1.1.3. N-Hexanol Hexanol (> 98%) was used as a cosurfactant for the formation of reversed micelles with Triton X-100. It was obtained from Fluka and used without further purification.

2.1.2. Nonpolar Solvents

2.1.2.1. Cyclohexane Cyclohexane was used in the formation of Triton X-100/ammonia/cyclohexane microemulsions. It was obtained from Ferak Berlin and used without any purification.

2.1.2.2. N-Decane N-Decane was used in the formation of AOT/ammonia/decane reversed micellar systems. It was supplied from Merck and used without further purification

2.1.2.3. N-Heptane N-Heptane served as the oil phase in the AOT/ammonia/heptane reversed micellar systems. It was supplied from Merck and used without further purification.

2.1.3. Ammonia solution

Ammonia solution (29 per cent, wt per cent) was obtained from Merck. It served both as a catalyst and as a water source in the reaction.

2.1.4. Deionized water

Deionized H₂O was used as the solvent for the preparation of samples for the UV-VIS, fluorescence and particle size measurements.

2.1.5. Absolute ethanol

Absolute ethanol (99 per cent) was obtained from Rectapur. It was added to break the microemulsion and to recover the particles. The particles were also washed several times with ethanol.

2.1.6. Fluorescent Dyes

2.1.6.1. Rhodamine 101. Rhodamine 101 was supplied from Fluka (see Figure 2.1). It was soluble in ammonia and used to dope the silica particles. Trimethyl rhodamine dye (TMR) is one of the most commonly used rhodamine dyes, especially used in doping procedures.

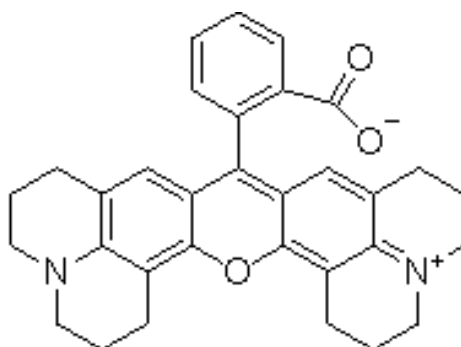


Figure 2. 1. The structure of Rhodamine 101 dye

2.1.6.2. Tris (2'2-bipyridine)ruthenium(II) chloride hexahydrate. The structure of dye, also called Ru(bipy)₃, is shown in Figure 2.2. It is an inorganic dye and it is the most commonly used dye in the preparation of dye-doped silica NPs in reversed micelles. It was supplied from Aldrich.

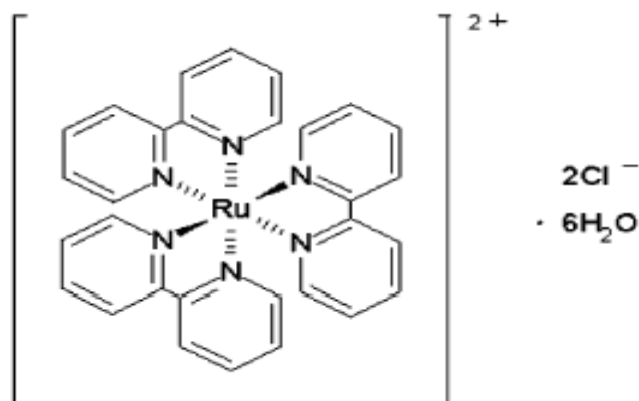


Figure 2. 2. The structure of Ru(bipy)₃ dye

2.1.6.3. Bodipy. Bodipy is the short notation for boron-dipyrromethene. It is remarkable for its sharp excitation and emission peaks, small Stokes shift and high environment-independent quantum yield. Its structure is shown in Figure 2.3. The bodipy dye used in this study was synthesized by Sanyal Research Group in the Department of Chemistry, Boğaziçi University.

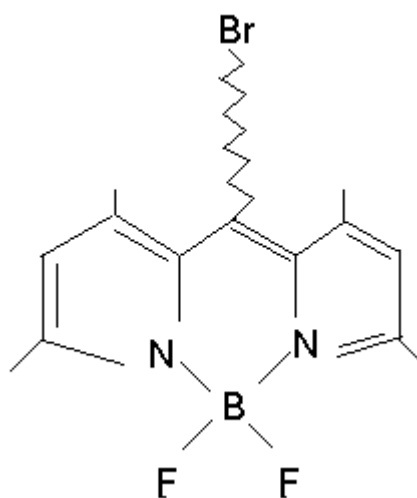


Figure 2. 3. The structure of Bodipy dye

2.1.7. Tetraethyl orthosilicate (TEOS)

TEOS was used in the silica NP synthesis as the silica precursor. It was supplied from Merck. Its structure is shown in Figure 2.4.

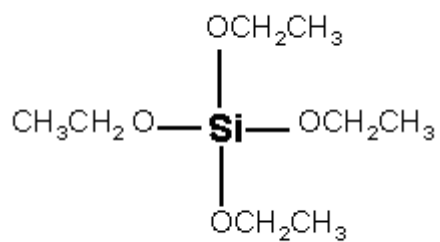


Figure 2. 4. The structure of TEOS

2.2.Instruments

2.2.1. Analytic Balance

AND GR-200 analytic balance was used.

2.2.2. Centrifuge

Rotafix 32 centrifuge with 4000RPM-6000RPM was used for recovering the solid silica NPs from the reversed micelles.

2.2.3. Sonicator

Banderin Sonorex sonicator was used to disperse the silica NPs in water.

2.2.4. Oven

An oven was used to remove residual organic solvents and ethanol from the silica NPs. The particles were left with top open overnight in the oven at 100 °C.

2.2.5. UV-VIS Spectrophotometer

UV-VIS measurements were done with the Shimadzu UV-1700 Spectrophotometer. All measurements were done with 1cm quartz cuvettes.

2.2.6. Fluorescence Spectrophotometer

The fluorescence properties of dye-doped silica NPs were measured on Perkin Elmer LS55 Luminescence spectrometer.

2.2.7. Particle Size Analyzer

To measure the particle size of silica NPs in the dispersed water droplets of reversed micelles and in water a Brookhaven Instruments 90 Plus Particle Size/Zeta Analyzer was used.

2.2.8. Scanning Electron Microscope

To determine the solid particle size a Philips XL30 ESEM-FEG/EDAX System was used.

2.2.9. Fourier Transform Infrared (FTIR) Spectrophotometer

The IR spectra of the silica NPs are taken with the Thermo Scientific Nicolet 380 FTIR Spectrometer.

3. EXPERIMENTAL METHODS

3.1. Preparation of AOT Stock Solution

For the preparation of AOT stock solution in n-heptane, required amount of AOT was placed into a beaker. N-Heptane was added to fill the solid part of the AOT. The beaker was sonicated in UV sonicator till the entire solid was dissolved. The sample was poured into a volumetric flask and the solution was filled with n-heptane up to the mark to obtain the required concentration. The same procedure was followed when preparing stock solution of AOT in n-decane.

3.2. Preparation of Dye Solutions

For the preparation of the stock solutions of fluorescent dyes, measured amounts of Rhodamine 101 dye, Ru(bipy)₃ dye and Bodipy dye were dissolved in required amount of ammonia solution.

3.3. Preparation Procedure of Silica NPs in Reversed Micelles

Silica NPs were prepared either in AOT-stabilized or Triton X-100-stabilized reversed micelles. Reactions were carried out in a 50 mL round bottom flask under nitrogen at room temperature.

3.3.1. AOT-stabilized Reversed Micelles

AOT-stabilized reversed micelles were prepared with R= 5, 7 and 10. The h, where $h=[\text{H}_2\text{O}]/[\text{TEOS}]$, was kept unchanged at 18.5 in all reversed micelles. The concentration of AOT was also kept constant at 1 M in all reversed micellar systems.

Initially, NH₃ (aq), which was the water source, was added into a round bottom flask. Then the measured amount of AOT in n-heptane or in n-decane was added from the stock solution. The solution became turbid at the beginning. Then n-heptane or n-decane was

added while magnetically stirring the solution. After a while, a transparent, thermodynamically stable solution was obtained. After 30 minutes, TEOS was added to the reversed micelles. The reaction solution was stirred for a further 24 hours. The reversed micelles were then broken down by the addition of ethanol and particles were recovered by centrifuging the solution. The solid particles were washed several times with ethanol to remove the solvents and the surfactant. The particles were left, with top open, overnight in the oven at 100 °C.

The above procedure was followed for the preparation of empty silica NPs (i.e. NPs with no dye in them). For the preparation of dye-doped ones, the dye solution was added in the first step instead of pure NH₃ (aq).

We obtained 40 to 50 per cent yield (30 mg) in production of the NPs.

3.3.2. Triton X-100-stabilized Reversed Micelles

When nonionic Triton X-100 was used as the surfactant, the procedure consisted of mixing 1.77 grams of Triton X-100, 1.6 mL of n-hexanol, 7.5 mL of cyclohexane, 0.4 mL of deionized water, 0.14 mL dye solution as suggested by Bagwe et al. [29]. After 30 minutes 0.1 mL of TEOS was added to the reaction solution. The reaction was stirred for 24 hours. By addition of ethanol, the reversed micelles were broken and particles were recovered by centrifuging the solution. The solid particles were then washed several times with ethanol to remove the solvents and the surfactant. The particles were left, with top open, overnight in the oven at 100 °C.

3.4. Scheme of the Reaction

The reaction scheme is shown in Figure 3.1. In the first step water-phase, (pure ammonia or dye solution), surfactant and oil-phase are mixed to form the reversed micelles. The dye enters the aqueous core of the reversed micelles. In the second and third steps, the reaction solution is stirred magnetically. NH₃ (aq) gives the OH⁻ ion which acts

as the base catalyst in the reaction. In the fourth step, after 30 minutes, TEOS is added to the reaction solution to react with water and be hydrolyzed to produce SiO₂, i.e. silica NPs.

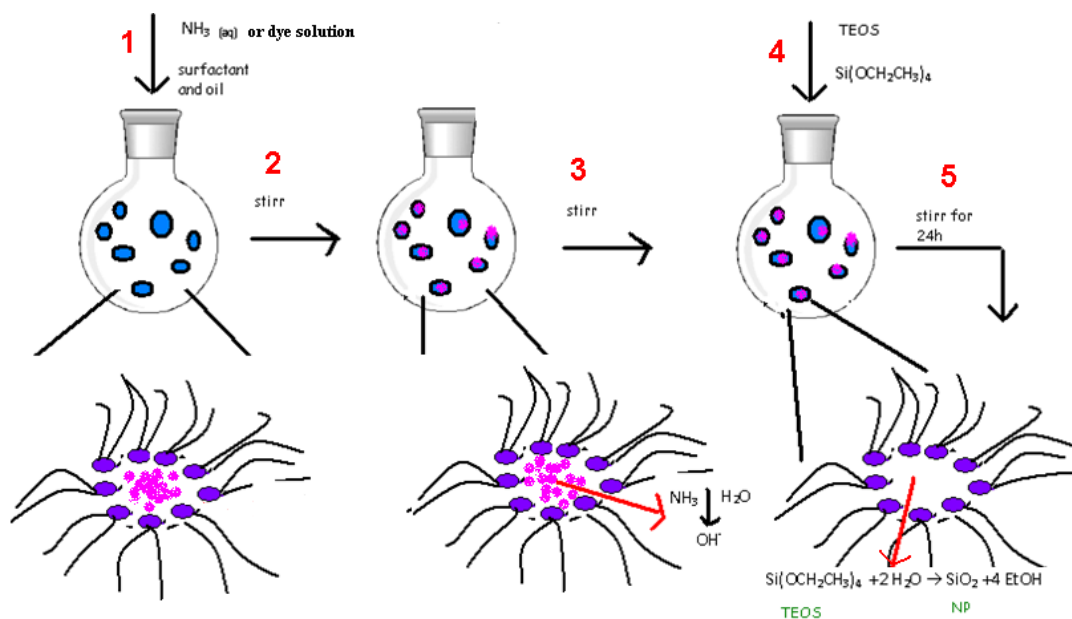


Figure 3. 1. Reaction Scheme

3.5. IR Measurements

IR measurements were taken between 400 cm⁻¹ and 4000 cm⁻¹ on solid silica NPs. Interpretation and the spectra are given in the Results and Discussion section.

3.6. Particle Size Measurements

To measure the particle size in the dispersed water droplets of reversed micelles, a 4 mL sample of the reaction solution was placed into the Brookhaven Instruments 90 Plus Particle Size/Zeta Analyzer. The scattering angle was kept 90° in all measurements. The effective diameter of the spherical silica NPs and the size distribution were determined. To

determine the size distribution, both lognormal distribution and multimodal size distributions (MSD) were used.

After the drying step, some samples were dispersed in deionized water (1 mg/2 mL) and sonicated for five hours. These solutions were used again to see the particle size of the silica NPs when dispersed in water. Then the solutions were kept without sonication. Size determination was carried out first after 24 hours, and then after five days. The results are given in the Results and Discussion section.

3.7. SEM Measurements

SEM measurements were carried out on solid particles. The particles were coated with gold before taking images. Accurate voltage was kept at 20kV in all measurements. Spot diameter was kept 3.0. A secondary electron detector was used, and the images were magnified 150000 times. SEM pictures are given in the Appendix section B.

3.8. UV/VIS Measurements

Absorbance measurements were performed by dispersing 1 mg/2 mL of the dye-doped silica NPs in deionized water. Absorption spectra of the pure dyes in aqueous media were also taken.

To see whether there were any differences before the addition of TEOS into the reaction mixture and after the formation of the particles, UV/VIS spectra of the Bodipy dye containing microemulsions were taken. All the results are shown in the Results and Discussion section.

3.9. Fluorescence Measurements

Fluorescence measurements were performed by dispersing 1 mg/2 mL of the dye-doped silica NPs in deionized water. Excitation wavelength for the emission spectra was 563 nm for Rhodamine 101-doped particles, 450 nm for the Ru(bipy)₃-doped particles and 503 nm for Bodipy-doped particles.

The emission spectra for the dye-doped silica NPs are given in the Results and Discussion section.

4. RESULTS AND DISCUSSIONS

4.1. General Remarks and Visual Observations

When preparing empty silica NPs, the formation of the particles were observed by the change of the color of the microemulsion. The microemulsion became bluish after four to six hours after the addition of TEOS. However, when preparing dye-doped silica NPs, this behavior could not be seen since the microemulsions had the color of the dye.

After centrifuging the solution, white solid particles were obtained when empty NPs were prepared. If dye-doped ones were being prepared, NPs had the color of the dye at the end. During the washing steps with ethanol, most of the dye passed into ethanol solution. To get rid of all the remaining dye on the surface of the particles, these washing steps were repeated until the ethanol solution was colorless.

Dispersion of the particles in water needed extended sonication (five hours). After one week, precipitation was observed in the aqueous solutions of the particles.

4.2. IR Results

The IR spectra of solid empty silica NP recovered from the AOT-stabilized reversed micelles were taken to confirm the production of silica NPs (Figure 4.1). The peaks at 450, 800, 1100 and 1600 cm^{-1} are in agreement with the peaks of amorphous silica in the literature (Figure 4.2) [29].

The IR spectra of dye-doped NPs were also taken, but very similar results were obtained. This showed no serious change in the particle structure due to doping. Since there was no change, these spectra were not included in this thesis.

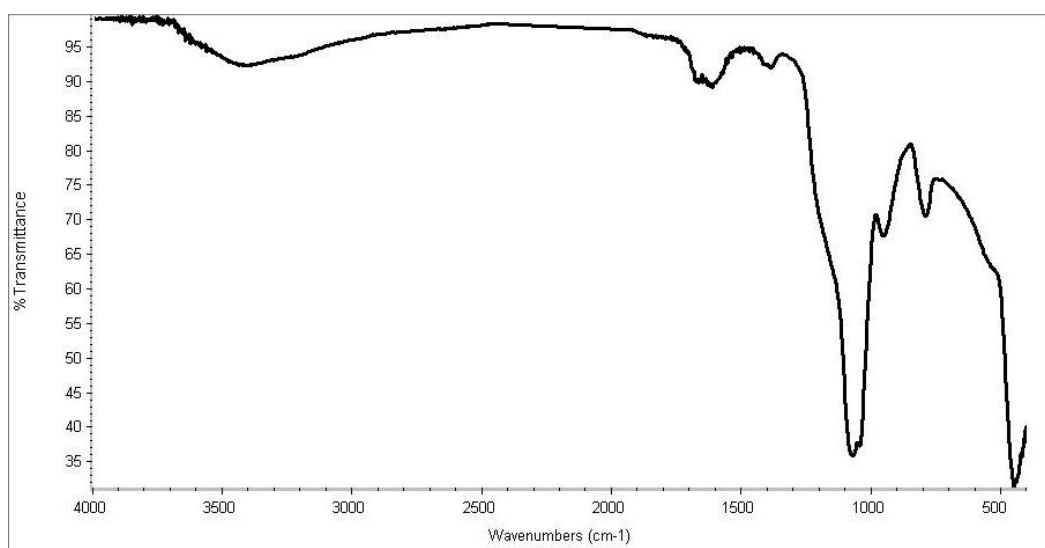


Figure 4. 1. The IR spectra of solid silica NPs recovered from AOT-stabilized reversed micelles

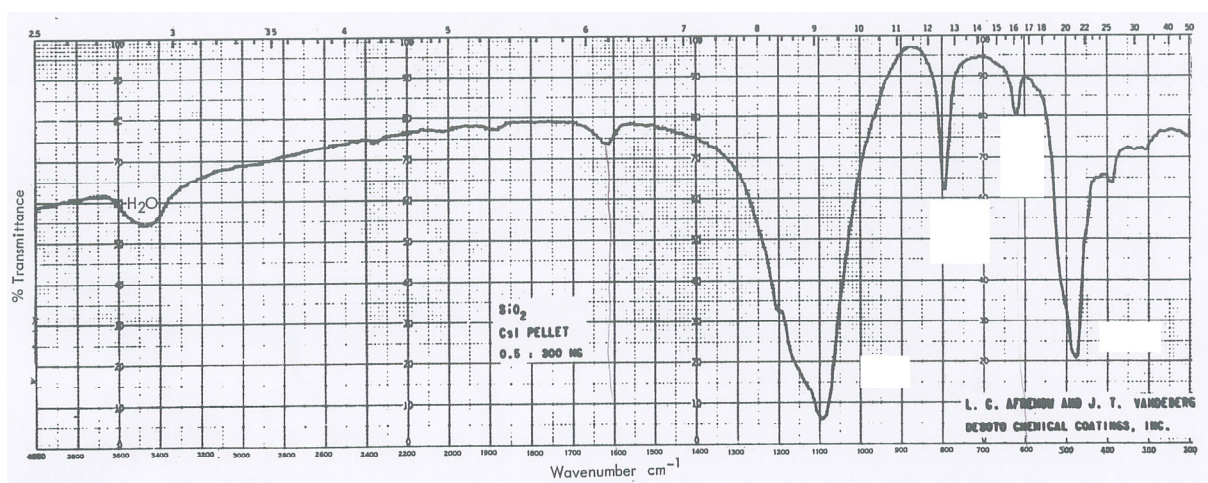


Figure 4. 2. The IR spectra of amorphous silica [30]

4.3. Particle Size Results

The results of 16 samples are given in the appendix sections A and B. Names, the type of the microemulsion they were synthesized in, R values and figure numbers of the samples are shown in the Table 4.1. The SEM results are not presented in the Table 4.1. They will be discussed in Table 4.3.

Table 4. 1. List of samples

Sample	Code of the sample	Type of the reversed micelles	R value	Name of the dye used	Particle Size/Zeta Analyzer picture	SEM picture	Effective Diameter*
S1	300108	AOT- stabilized NH ₃ (aq)/heptane	5	Without dye	Figure A.1	Figure B.1	66.2 nm
S2	040308-5	AOT- stabilized NH ₃ (aq)/heptane	5	Without dye	Figure A.2		60.2 nm
S3	280208	AOT- stabilized NH ₃ (aq)/heptane	7	Without dye	Figure A.3	Figure B.2	76.9 nm
S4	110308-10	AOT- stabilized NH ₃ (aq)/heptane	10	Without dye	Figure A.4	Figure B.3	84.5 nm
S5	110608 R5	AOT- stabilized NH ₃ (aq)/heptane	5	Rhodamine 101	Figure A.5		78.1 nm
S6	110608 R7	AOT- stabilized NH ₃ (aq)/heptane	7	Rhodamine 101	Figure A.6	Figure B.4	98.8 nm
S7	070408-10rh	AOT- stabilized NH ₃ (aq)/heptane	10	Rhodamine 101	Figure A.7		111.2 nm
S8	080408-TR	Triton X-100- stabilized NH ₃ (aq)/cyclohexane		Rhodamine 101	Figure A.8	Figure B.5	235 nm
S9	170608-5	AOT- stabilized NH ₃ (aq)/heptane	5	Ru(bipy) ₃		Figure B.6	
S10	170608-7	AOT- stabilized NH ₃ (aq)/heptane	7	Ru(bipy) ₃	Figure A.9	Figure B.7	80.4 nm
S11	170608-10	AOT- stabilized NH ₃ (aq)/heptane	10	Ru(bipy) ₃	Figure A.10	Figure B.8	84.2 nm
S12	240608TRW	Triton X-100 – stabilized NH ₃ (aq)/cyclohexane		Ru(bipy) ₃		Figure B.9	
S13	070708-5D	AOT- stabilized NH ₃ (aq)/heptane	5	Bodipy	Figure A.11	Figure B.10	54.7 nm
S14	300608-7	AOT – stabilized NH ₃ (aq)/heptane	7	Bodipy	Figure A.12	Figure B.11	88.1 nm
S15	210708-10W	AOT- stabilized NH ₃ (aq)/heptane	10	Bodipy	Figure A.13	Figure B.12	93.2 nm
S16	070708-TRW	Triton X-100- stabilized NH ₃ (aq)/cyclohexane		Bodipy	Figure A.14	Figure B.13	86 nm

*Measured by Particle Size/Zeta Analyzer (The missing values attributed to very low droplet concentrations.)

The size results for the empty silica nanoparticles, prepared in AOT-stabilized reversed micelles, show that the particle size increases with increasing R value. This trend is in agreement with the observation of Osseo-Assare and Arrigada [23]. The particle size values we have observed from the Particle Size/Zeta Analyzer are compared with those reported by Osseo-Assare and Arrigada by using TEM (Table 4.2). It can be clearly observed that the values for the AOT-stabilized systems obtained from two different methods are very different.

Table 4. 2. Particle size values compared with the values in literature

Sample in this work	R value	Particle Size/Zeta Analyzer Values After 26 hours	TEM values from literature[22] after 18 hours
S2	5	60.2 nm	12.5 nm
S3	7	76.9 nm	22.5 nm
	9.5		35 nm
S4	10	84.5 nm	

Although there is a significant difference in sizes of the NPs, the 80 per cent increase, observed by Osseo-Assare and Arrigada in going from R=5 to R=7, is reduced to 28 per cent increase in our systems. Hence the effect of 40 per cent increase in the core radius when R is changed from 5 ($r_{\text{core}}=0.875$ nm) to 7 ($r_{\text{core}}=1.225$ nm) does not have the same dramatic effect of almost doubling the NP size. In our studies when R increases to 10, so $r_{\text{core}}=1.75$ nm, the size of the NPs increases by 40 per cent, still a much less increase compared to Osseo-Assare and Arrigada, when the water droplet core size is doubled. Nevertheless, the trend of size-increase is similar in both cases.

There was no significant difference in the particle size when the nonpolar solvent of the system was changed from n-heptane to n-decane (S1 and S2). For the AOT-stabilized reversed micelles with R=5, the determined particle size was 66.2 nm and 60.2 nm when the oil phase was n-heptane and n-decane, respectively.

When the effect of doping on the sizes of the NPs was considered, in the case of NPs prepared in AOT-stabilized systems, Rhodamine 101-doped NPs showed up to 30% size increase (Table 4.3). This size increase was up to 10% for Bodipy-doped NPs. Not so different results were obtained for NPs doped with Ru(bipy)₃. This show a successful

doping with Ru(bipy)₃. Because of the hydrophilic nature of Ru(bipy)₃, it can enter the core of the water droplets of reversed micelles and hence it can be entrapped into the silica matrix and hence the size doesn't change. With the other two dyes (Rhodamine 101 and Bodipy), because of the more hydrophobic nature of the dyes, they are more likely to be on the interface of the reversed micelles. Hence the entrapment into the silica matrix is poorer. This is, in fact, in agreement with the observations which will be discussed further on.

Table 4. 3. Particle size values for empty and doped NPs

Sample in this work	Type of reversed micelles	R value	Type of the silica NPs	Effective diameter (nm)
S1	AOT-stabilized	5	Empty	66.2
S5			Rhodamine-doped	78
S9			Ru(bipy) ₃ -doped	
S13			Bodipy-doped	54.7
S3	AOT-stabilized	7	Empty	76.9
S6			Rhodamine-doped	98
S10			Ru(bipy) ₃ -doped	80.4
S14			Bodipy-doped	88.1
S4	AOT-stabilized	10	Empty	84.5
S7			Rhodamine-doped	112
S11			Ru(bipy) ₃ -doped	84.2
S15			Bodipy-doped	93.2

Three dye-doped samples (S10, S11 and S16) were chosen for further analysis. Ten particles from each of these samples were taken and the particle size analysis was carried out using SEM (Figure B.7, Figure B.8 and Figure B.13). These SEM results were then compared with the Particle Size/Zeta Analyzer results (see Table 4.4).

Table 4. 4. Particle Size Comparison

Sample	Type of the reversed micelles	Type of the silica NPs	R value	Particle size measured using SEM (mean of 10 particles sizes)	Effective diameter measured using Particle Size/Zeta Analyzer
S10	AOT-stabilized	Ru(bipy) ₃ -doped	7	55.96 nm	80.4 nm
S11	AOT-stabilized	Ru(bipy) ₃ -doped	10	72.07 nm	84.2 nm
S16	Triton X-100-stabilized	Bodipy-doped		71 nm	86 nm

It can be seen that the SEM values are 12 to 25 per cent smaller than the Particle Size/Zeta Analyzer results. This might be also account for the size differences we observe by Particle Size/Zeta Analyzer when compared with those reported in literature [23]. In other words, different methods show different sizes. It might depend on the preparation of the samples. The NPs were in the reversed micelles or were dispersed in aqueous media when measuring the particle size with Particle Size/Zeta Analyzer. The principle of Particle Size/Zeta Analyzer is based on Dynamic Light Scattering. The measurements were done at a scattering angle 90° . The solutions were scanned ten times for each measurement and the effective diameter is then calculated from these ten measurements automatically. The NPs were in solid form when SEM analysis was done. From the produced SEM image, ten particles were chosen randomly and the sizes were measured and then the mean of these ten values was calculated. The SEM image presents only one part of the solid sample, so one can not be sure whether this image is all the same for whole sample. However, in Particle Size/Zeta Analyzer a wider region of the solution was scanned.

SEM results show that the particles are in spherical shapes. The size distribution range is much larger for S9-S11 (i.e. for AOT-stabilized systems) with respect to S8, S12 and S16 (i.e. Triton X-100-stabilized systems). The NPs are more uniform (i.e. monodispersed) when the surfactant is Triton X-100 (Figure B.5, Figure B.9, and Figure B.13). This trend was also observed by Osseo-Assare and Arrigada [23]. The maximum and

minimum particle size values measured by SEM when using Triton X-100 or AOT as surfactant are given in Table 4.5.

Table 4. 5. Minimum and maximum particle size values measured with SEM

Sample	Surfactant used	Minimum particle size (nm)	Maximum particle size (nm)	% Difference
S9	AOT	54.54	86.99	59
S10		49.85	73.78	48
S11		63.06	76.47	21
S8	Triton X-100	63.37	78.47	23
S12		53.03	64.48	21
S16		63.10	82.08	30

NPs recovered from S14 and S10 were dried and then dispersed in aqueous media in order to check their stability. The sizes measured are as follows:

Table 4. 6. Particle size values in aqueous media

Sample	Immediately after dispersion	After 25hours	After 5days
S10	80.4 nm	85 nm	
S14		85.2 nm	84.4 nm

As seen from Table 4.6 the particles are quite stable and there is no significant size change with time. The same results can be also seen from Figure A.15-A.18 in the appendix section A.

4.4 UV/VIS and Fluorescence Results

4.4.1. Results for Ru(bipy)₃-doped Silica NPs

The purpose of taking the UV/VIS spectra of the dye-containing solutions was to see the λ_{\max} of the dye in a given system and able to use this value as the excitation wavelength in fluorescence emission spectra. Figure 4.3 is the absorbance spectrum of pure Ru(bipy)₃ in aqueous solution. The λ_{\max} appears at 450 nm.

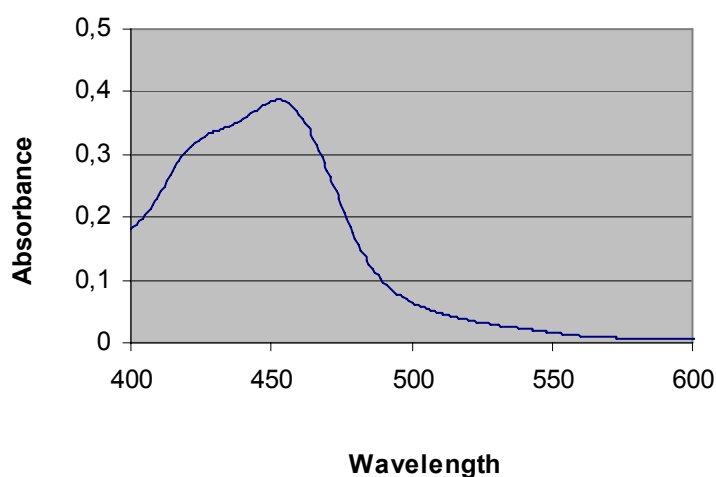


Figure 4. 3. Absorbance versus wavelength plot of Ru(bipy)₃ in water

The spectrum obtained by dispersing the Ru(bipy)₃-doped silica NPs, prepared in AOT-stabilized reversed micelles, in aqueous media is shown in Figure 4.4. A very slight hump for both samples S10 and S11 are seen at the same wavelength (i.e. 450 nm).

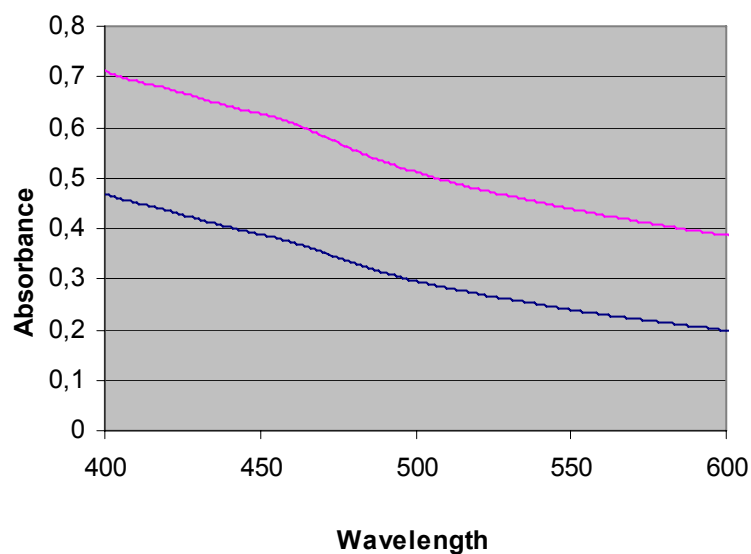


Figure 4. 4. Absorbance versus wavelength plot of sample S10 (blue) and S11 (pink) in aqueous media

However when a similar spectrum was taken for the particles recovered from Triton X-100-stabilized systems (Figure 4.5), a clear λ_{\max} was seen in the same position as the pure dye case (i.e. Figure 4.3).

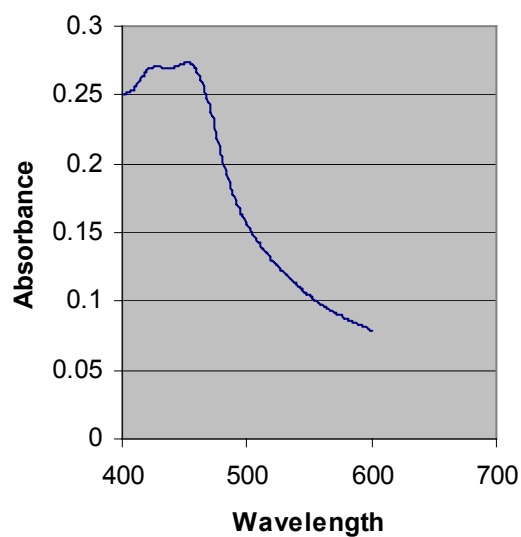


Figure 4. 5. Absorbance versus wavelength plot of sample S12 in aqueous media

Having obtained the λ_{max} of the dye, the fluorescence emission spectra of the samples were run at an excitation wavelength 450 nm.

The results for pure dye, dye-doped NPs prepared in AOT-stabilized droplets of various R values (S9-S11) are seen in Figure 4.6. The result for the dye-doped NPs prepared in Triton X-100-stabilized droplets (S12) is seen in Figure 4.7.

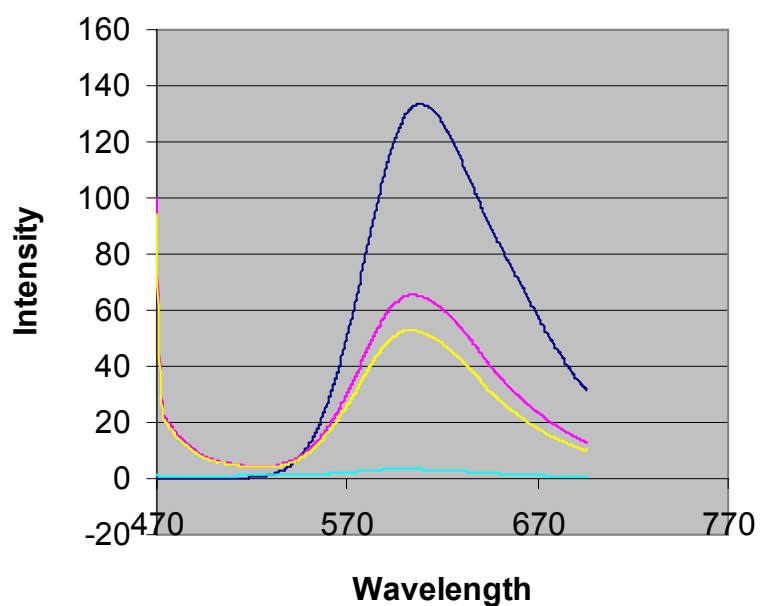


Figure 4. 6. Fluorescence emission spectra of pure Ru(bipy)₃ (blue), sample S11 (pink), S10 (yellow) and S9 (green) in aqueous media

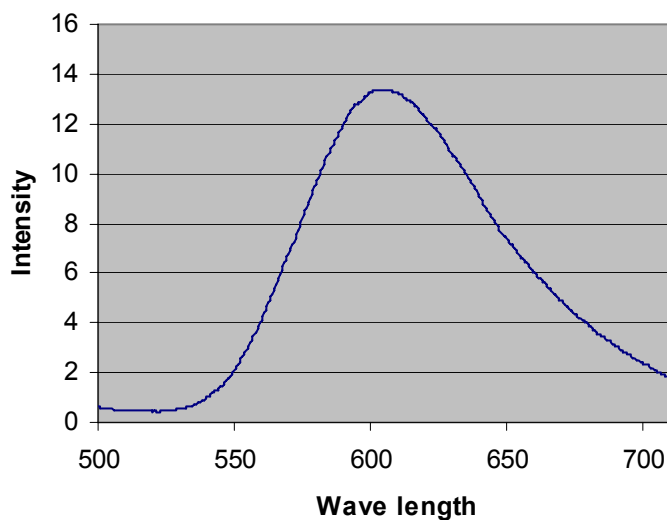


Figure 4. 7. Fluorescence emission spectra of sample S12 in aqueous media

The λ_{\max} of fluorescence emission spectra of pure Ru(bipy)₃ dye in aqueous media is at 605.5 nm. The λ_{\max} values of the Ru(bipy)₃-doped silica NPs dispersed in aqueous media are located in a different position. It is 593 nm for sample S9 prepared in AOT-stabilized droplets of R=5, 604 nm for sample S10 prepared in AOT-stabilized droplets of R=7 and 604,5 nm for S11 prepared in AOT-stabilized droplets of R=10. The λ_{\max} value of the sample S12, which was prepared in Triton X-100-stabilized reversed micelles, is at 604 nm.

As seen in Figure 4.6 the intensities increase by increasing R value, i.e. increasing particle size. The intensity observed from the spectrum of S12 prepared in Triton X-100-stabilized reversed micelles is lower than those prepared in AOT-stabilized reversed micelles with R=7 (S10) and R=10 (S11) but higher than those with R=5 (S9).

4.4.2. Results for Rhodamine 101-doped Silica NPs

UV/VIS spectra of the Rhodamine 101-doped silica NPs were taken. Even though aqueous solution of pure Rhodamine 101 dye gave a peak at 563nm (Figure 4.8), no absorption peak has been observed for Rhodamine 101-doped silica NPs dispersed in aqueous media.

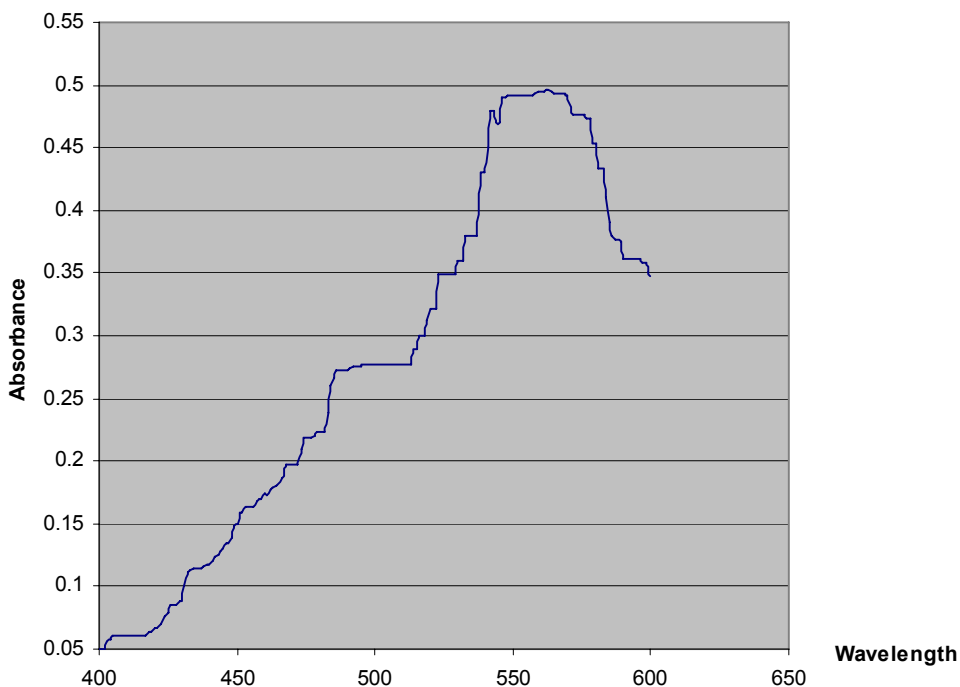


Figure 4. 8. Absorbance versus wavelength plot of pure Rhodamine 101 dye in aqueous media

Furthermore, no peaks were observed in the fluorescence emission spectra for the pure Rhodamine 101 dye in aqueous media, or for the Rhodamine 101-doped silica NPs dispersed in aqueous media.

Having seen no peaks, the excitation λ , the concentration of the dye and the concentration of the particles have been altered, but still no results could be obtained, even for the pure dye in aqueous media. This was a highly surprising result, considering the fluorescent nature of the dye. Having thought that might have been a solvent effect, pure dye was studied in methanol as suggested by Fluka. This change of solvent was as unsuccessful.

The reason for choosing Rhodamine 101 dye was because Roy et al. had used organically modified silica (ORMOSIL) NPs doped with a similar Rhodamine dye, Rhodamine 6G, in labeling DNA [31]. However, they had used another system for the

synthesis. They synthesized the ORMOSIL NPs in the apolar core of the AOT-stabilized normal micelles. Their doping was a successful one.

The reason for not observing the entrapment of the Rhodamine 101 dye into the silica NPs might be due to the amphiphilic nature of the dye. Probably, the dye was not hydrophilic enough to enter the core of reversed micelles and needs to be modified to do so.

4.4.3. Results for Bodipy-doped Silica NPs

The UV/VIS spectrum of Bodipy in $\text{NH}_3(\text{aq})$ has a sharp peak at 500 nm (Figure 4.9).

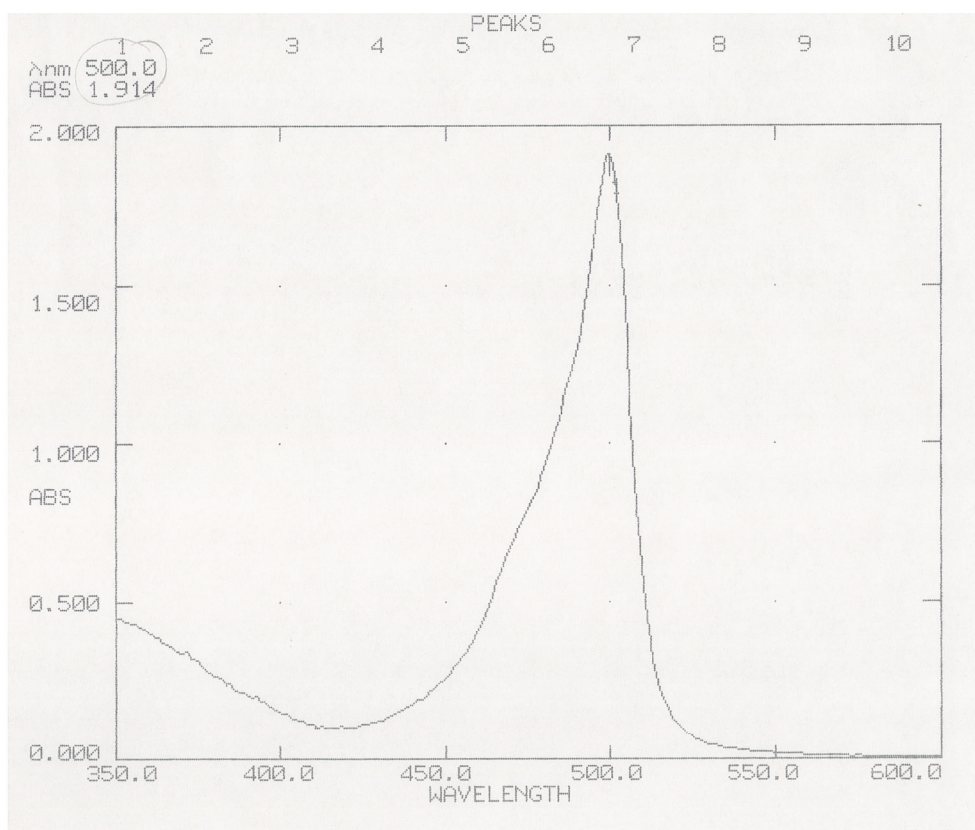


Figure 4. 9. Absorbance versus wavelength plot of pure bodipy dye in $\text{NH}_3(\text{aq})$

When the UV/VIS spectrum of silica NPs doped with Bodipy was studied, there was no absorbance peak in this region.

Similarly, when the fluorescence spectra of pure dye and the dye-doped silica NPs were run, no peak could be observed. The excitation λ , the concentration of the dye and the particles, the solvent, in which the dye and the silica NPs were dispersed have been altered, but still no peak was observed. The results were similar to Rhodamine 101 case.

This result also confirms that the nature of the dye should be more hydrophilic to dope the unmodified silica NPs using reversed micellar systems. Further work should be done with these hydrophobic dyes and probably modification could help with the doping process.

5. CONCLUSION

In this study both empty and dye-doped silica NPs were synthesized in reversed micellar systems stabilized with an anionic surfactant, AOT, and with a nonionic surfactant, Triton X-100. The NPs were doped with three different types of fluorescent dyes; Rhodamine 101, Ru(bipy)₃ and Bodipy.

The particles were characterized by their size and by their fluorescent properties.

It has been observed that the size of the NPs can be controlled by changing the water-to-surfactant molar ratio, i.e. the droplet size. As the droplet size increases the size of the NPs also increases. By characterizing the NPs by SEM, it has been observed that the particles have spherical and uniform shapes. The particles were more monodispersed when they were prepared by using Triton X-100 as the surfactant. When the particles were dispersed in water and kept five days without sonication, the size of the particles didn't change significantly which shows their stability.

Aqueous solution of Ru(bipy)₃-doped silica NPs showed peak in the fluorescence emission spectra proving a highly successful doping process. Silica NPs doped with amphiphilic Rhodamine 101 and hydrophobic Bodipy dye showed no peaks in the fluorescence emission spectra. This results showed the necessity of using either hydrophilic or hydrophilically modified dyes in order to dope the silica NPs prepared by reversed micellar systems.

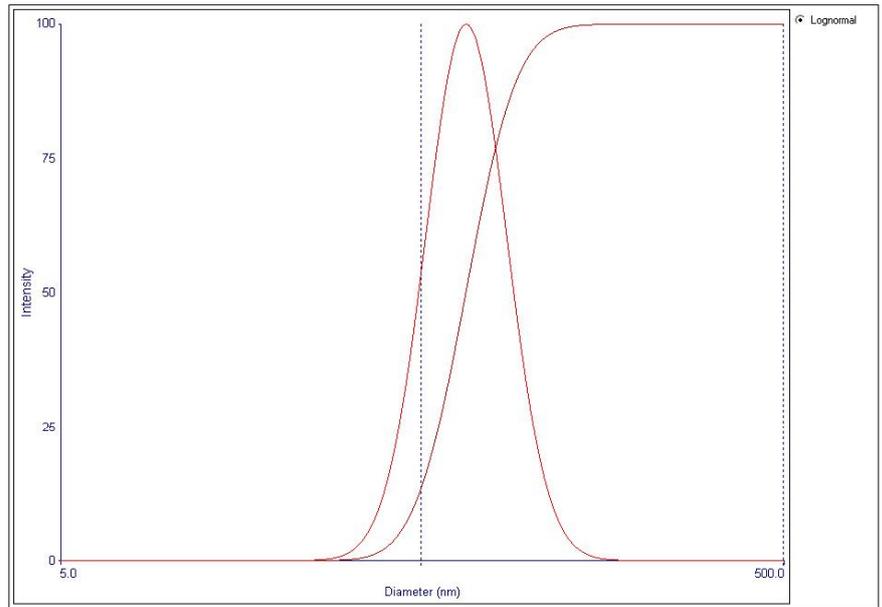
6. SUGGESTIONS FOR FUTURE WORK

1. The process for the entrapment of Rhodamine 101 and Bodipy dye should be improved. Dyes should be modified so that they would be more hydrophilic.
2. Fluorescence emission spectra of the pure Rhodamine 101 and Bodipy dye should be observed in apolar media.
3. The entrapment efficiency and the release kinetics of the dyes from the Silica NPs should be determined.
4. In order to use fluorescent dye-doped silica NPs in specific biomolecule detection, the surface of the Silica NPs should be modified with various functional groups.
5. The surface area of the NPs produced can be determined by using BET Instrument.

APPENDIX A: THE PARTICLE SIZE ANALYZER RESULTS

The following pages (47-62) present the results for the particle size analyzer.

300108 (Combined)
Effective Diameter: 66.2 nm
Polydispersity: 0.068
Avg. Count Rate: 343.1 kcps
Baseline Index: 2.7/ 98.40%
Elapsed Time: 00:10:00



Run	Eff. Diam. (nm)	Half Width (nm)	Polydispersity	Baseline Index
1	66.2	19.3	0.085	9.6/100.00%
2	66.7	17.3	0.067	8.0/100.00%
3	66.4	19.5	0.086	8.7/95.56%
4	66.7	17.5	0.069	9.7/100.00%
5	66.1	17.4	0.069	9.6/100.00%
6	65.0	19.3	0.088	7.6/95.56%
7	66.8	16.5	0.061	7.7/100.00%
8	66.0	17.0	0.066	9.5/100.00%
9	65.9	17.7	0.072	9.2/100.00%
10	65.9	15.8	0.058	9.5/92.89%
Mean	66.2	17.7	0.072	8.9/98.40%
Std. Error	0.2	0.4	0.003	0.3/0.85
Combined	66.2	17.3	0.068	2.7/98.40%

Sample ID 300108 (Combined)
 Operator ID sinan
 Elapsed Time 00:10:00
 Mean Diam. 71.0 nm
 Rel. Var. 0.118
 Skew 0.686

d(nm)	G(d)	C(d)	d(nm)	G(d)	C(d)	d(nm)	G(d)	C(d)
2.2	0	0	39.5	36	12	717.1	0	100
2.8	0	0	51.4	72	34	933.3	0	100
3.7	0	0	66.9	100	65	1214.7	0	100
4.8	0	0	87.1	72	87	1580.9	0	100
6.2	3	1	113.4	36	98	2057.5	0	100
8.1	0	1	147.5	6	100	2677.9	0	100
10.6	0	1	192.0	0	100	3485.2	0	100
13.8	0	1	249.9	0	100	4536.0	0	100
17.9	0	1	325.3	0	100	5903.6	0	100
23.3	0	1	423.3	0	100	7683.5	0	100
30.4	0	1	551.0	0	100	10000.0	0	100

Figure A. 1. Particle size data of sample S1

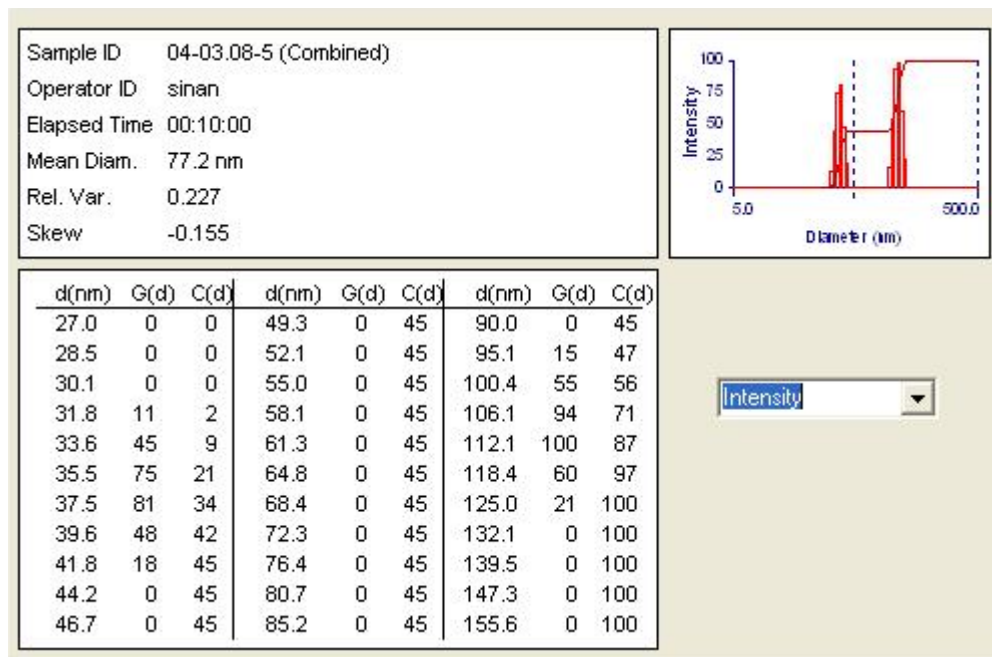
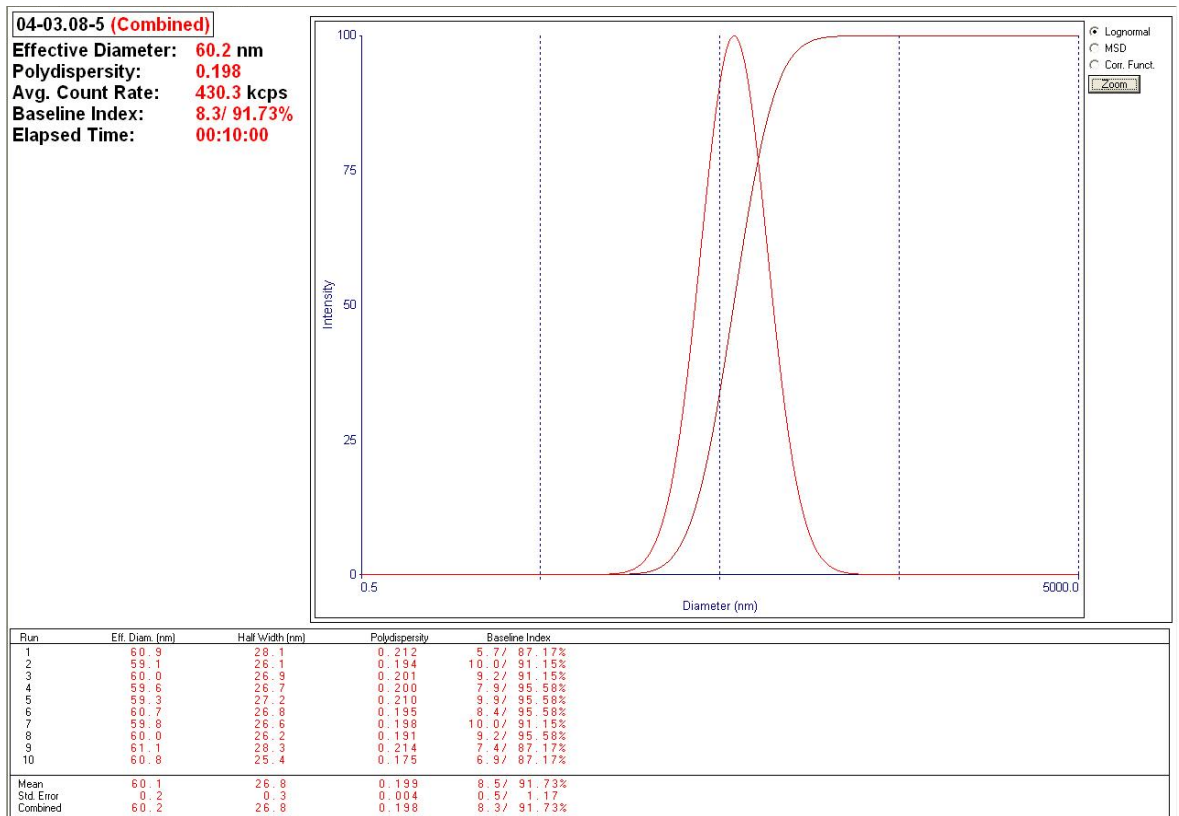


Figure A. 2. Particle size data of sample 040308-5

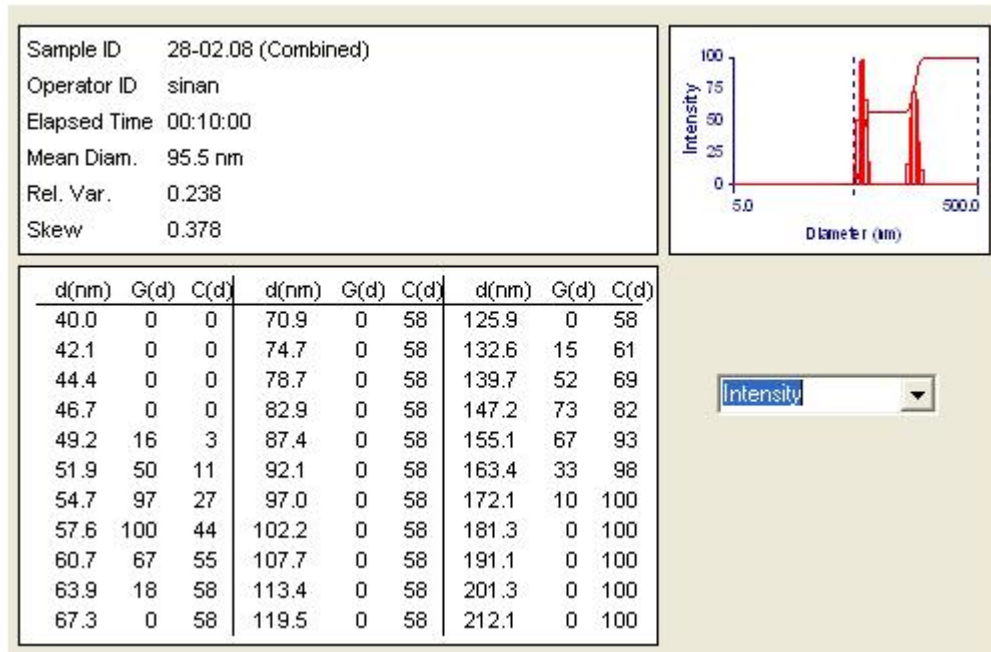
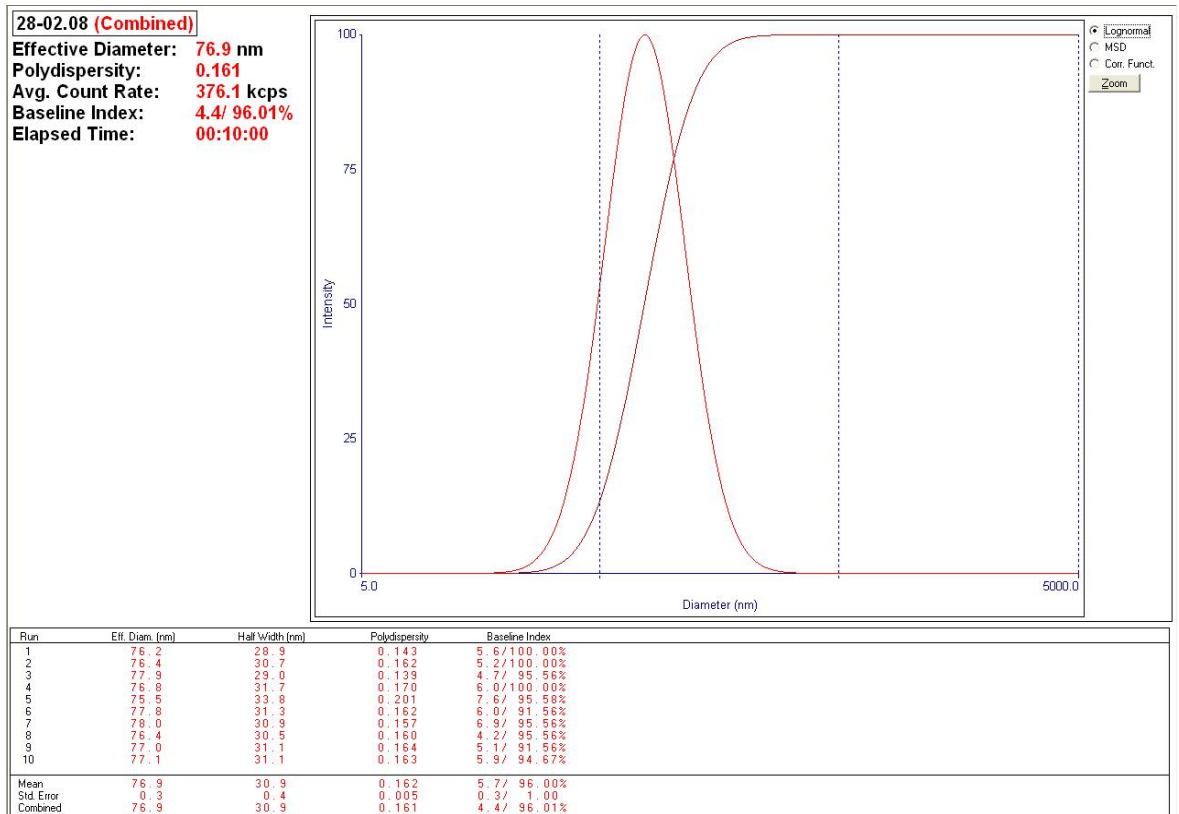
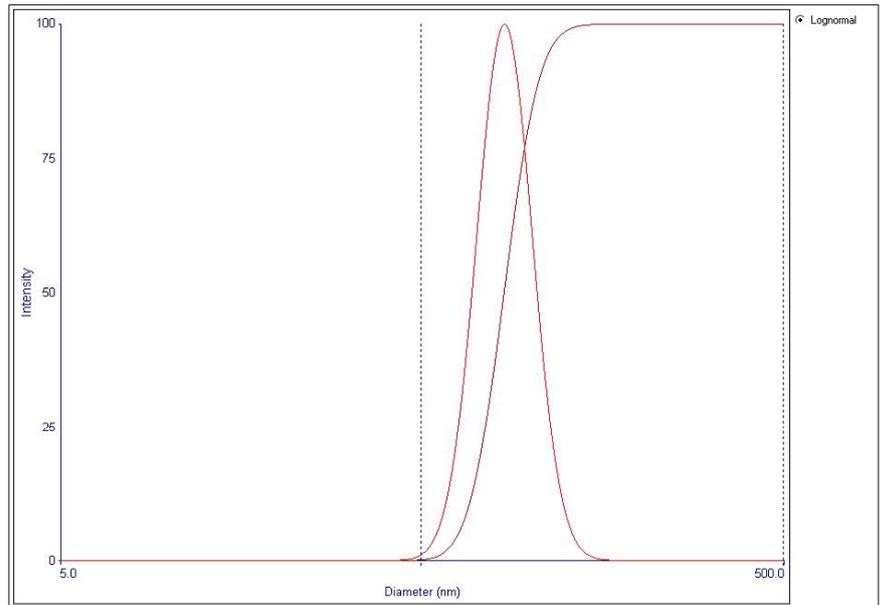


Figure A. 3. Particle size data of sample S3

11-03-08-10 (Combined)

Effective Diameter: 84.5 nm
 Polydispersity: 0.032
 Avg. Count Rate: 389.8 kcps
 Baseline Index: 9.0/100.00%
 Elapsed Time: 00:10:00



Run	Eff. Diam. (nm)	Half Width (nm)	Polydispersity	Baseline Index
1	83.2	15.7	0.036	8.6/100.00%
2	85.0	6.0	0.005	9.9/100.00%
3	83.9	19.3	0.053	8.5/100.00%
4	84.7	16.1	0.036	7.6/100.00%
5	84.1	22.3	0.070	7.9/100.00%
6	84.1	10.4	0.015	9.4/100.00%
7	85.0	18.6	0.048	8.1/100.00%
8	84.7	13.4	0.025	9.5/100.00%
9	84.9	17.3	0.041	9.6/100.00%
10	84.0	17.7	0.044	9.9/100.00%
Mean	84.4	15.7	0.037	8.9/100.00%
Std. Error	0.2	1.5	0.006	0.3/ 0.00
Combined	84.5	15.0	0.032	9.0/100.00%

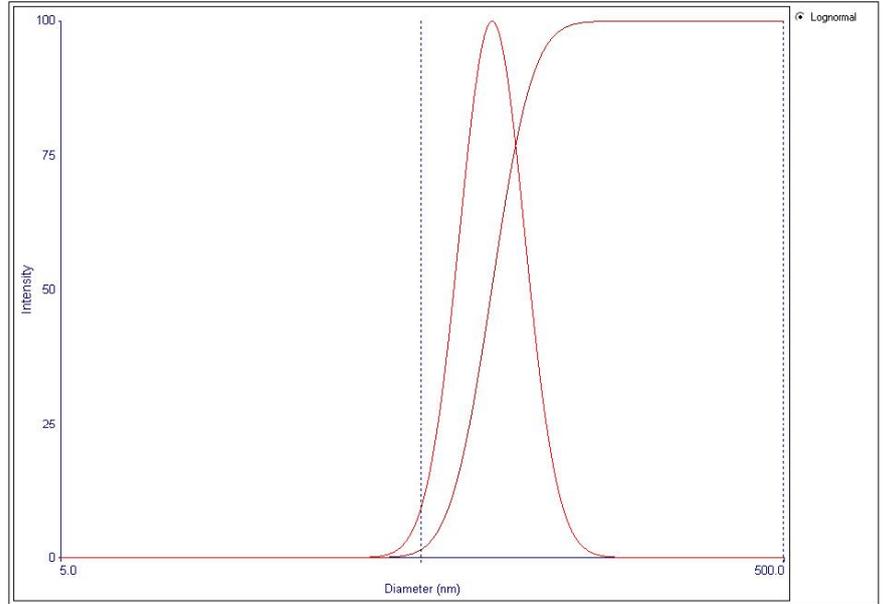
Sample ID 11-03-08-10 (Combined)
 Operator ID sinan
 Elapsed Time 00:10:00
 Mean Diam. 86.0 nm
 Rel. Var. 0.000
 Skew 0.006

d(nm)	G(d)	C(d)	d(nm)	G(d)	C(d)	d(nm)	G(d)	C(d)
83.2	0	0	85.1	0	0	87.0	0	100
83.4	0	0	85.4	52	7	87.2	0	100
83.6	0	0	85.5	69	17	87.4	0	100
83.7	0	0	85.7	85	29	87.5	0	100
83.9	0	0	85.8	96	43	87.7	0	100
84.1	0	0	86.0	100	57	87.9	0	100
84.2	0	0	86.1	96	71	88.1	0	100
84.4	0	0	86.3	85	83	88.3	0	100
84.6	0	0	86.5	69	93	88.4	0	100
84.7	0	0	86.6	52	100	88.6	0	100
84.9	0	0	86.8	0	100	88.8	0	100

Figure A. 4. Particle size data of sample S4

11-06-08 R5 (Combined)

Effective Diameter: **78.1 nm**
 Polydispersity: **0.044**
 Avg. Count Rate: **290.6 kcps**
 Baseline Index: **9.8/ 99.55%**
 Elapsed Time: **00:10:00**



Run	Eff. Diam. (nm)	Half Width (nm)	Polydispersity	Baseline Index
1	78.6	13.8	0.031	9.6/100.00%
2	77.6	18.1	0.055	9.6/100.00%
3	77.3	20.2	0.068	9.5/100.00%
4	78.5	17.2	0.048	9.8/ 99.56%
5	78.1	17.8	0.052	9.8/100.00%
6	77.5	23.5	0.092	8.9/100.00%
7	78.1	11.0	0.020	9.2/100.00%
8	78.2	16.6	0.045	9.7/100.00%
9	77.7	9.0	0.013	8.5/100.00%
10	78.5	15.9	0.041	9.6/100.00%
Mean	78.0	16.3	0.046	9.4/ 99.56%
Std. Error	0.1	1.3	0.007	0.1/ 0.44
Combined	78.1	16.3	0.044	9.8/ 99.55%

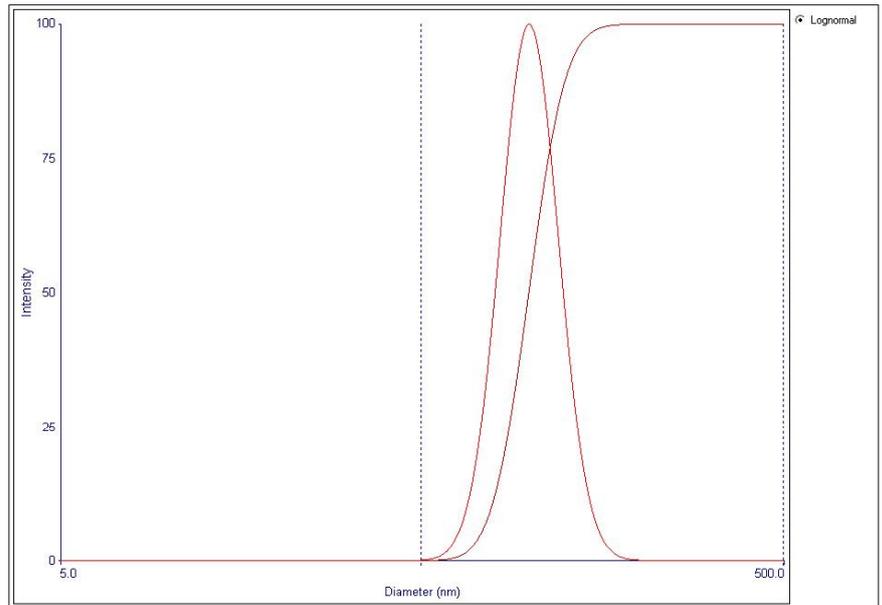
Sample ID 11-06-08 R5 (Combined)
 Operator ID sinan
 Elapsed Time 00:10:00
 Mean Diam. 80.1 nm
 Rel. Var. 0.000
 Skew -0.007

d(nm)	G(d)	C(d)	d(nm)	G(d)	C(d)	d(nm)	G(d)	C(d)
77.6	0	0	79.3	0	0	80.9	0	100
77.8	0	0	79.4	0	0	81.1	0	100
77.9	0	0	79.6	0	0	81.2	0	100
78.1	0	0	79.7	17	5	81.4	0	100
78.2	0	0	79.9	57	21	81.6	0	100
78.4	0	0	80.0	96	48	81.7	0	100
78.5	0	0	80.2	100	77	81.9	0	100
78.7	0	0	80.3	61	94	82.0	0	100
78.8	0	0	80.5	21	100	82.2	0	100
79.0	0	0	80.6	0	100	82.3	0	100
79.1	0	0	80.8	0	100	82.5	0	100

Figure A. 5. Particle size data of sample S5

11-06-08 R7 (Combined)

Effective Diameter: **98.8 nm**
 Polydispersity: **0.035**
 Avg. Count Rate: **363.6 kcps**
 Baseline Index: **9.9/100.00%**
 Elapsed Time: **00:10:00**



Run	Eff. Diam. (nm)	Half Width (nm)	Polydispersity	Baseline Index
1	98.6	3.1	0.001	9.7/100.00%
2	97.0	28.6	0.087	8.8/100.00%
3	99.1	18.7	0.036	9.5/100.00%
4	99.5	19.6	0.035	9.1/100.00%
5	100.1	10.9	0.012	9.3/100.00%
6	99.5	17.6	0.032	8.6/100.00%
7	97.7	19.5	0.040	9.7/100.00%
8	96.9	27.3	0.080	9.1/100.00%
9	98.6	29.5	0.089	9.3/100.00%
10	99.5	9.5	0.009	9.6/100.00%
Mean	98.5	18.3	0.042	9.3/100.00%
Std. Error	0.3	2.7	0.010	0.1/ 0.00
Combined	98.8	18.4	0.035	9.9/100.00%

Sample ID 11-06-08 R7 (Combined)
 Operator ID sinan
 Elapsed Time 00:10:00
 Mean Diam. 99.9 nm
 Rel. Var. 0.000
 Skew -0.581

d(nm)	G(d)	C(d)	d(nm)	G(d)	C(d)	d(nm)	G(d)	C(d)
96.8	0	0	99.0	15	4	101.2	0	100
97.0	0	0	99.2	27	9	101.5	0	100
97.2	0	0	99.4	43	16	101.7	0	100
97.4	0	0	99.6	62	26	101.9	0	100
97.6	0	0	99.8	81	39	102.1	0	100
97.8	0	0	99.9	95	55	102.3	0	100
98.0	0	0	100.1	100	71	102.5	0	100
98.2	0	0	100.3	95	87	102.7	0	100
98.5	0	0	100.5	81	100	102.9	0	100
98.6	4	1	100.8	0	100	103.1	0	100
98.8	8	2	101.0	0	100	103.3	0	100

Figure A. 6. Particle size data of sample S6

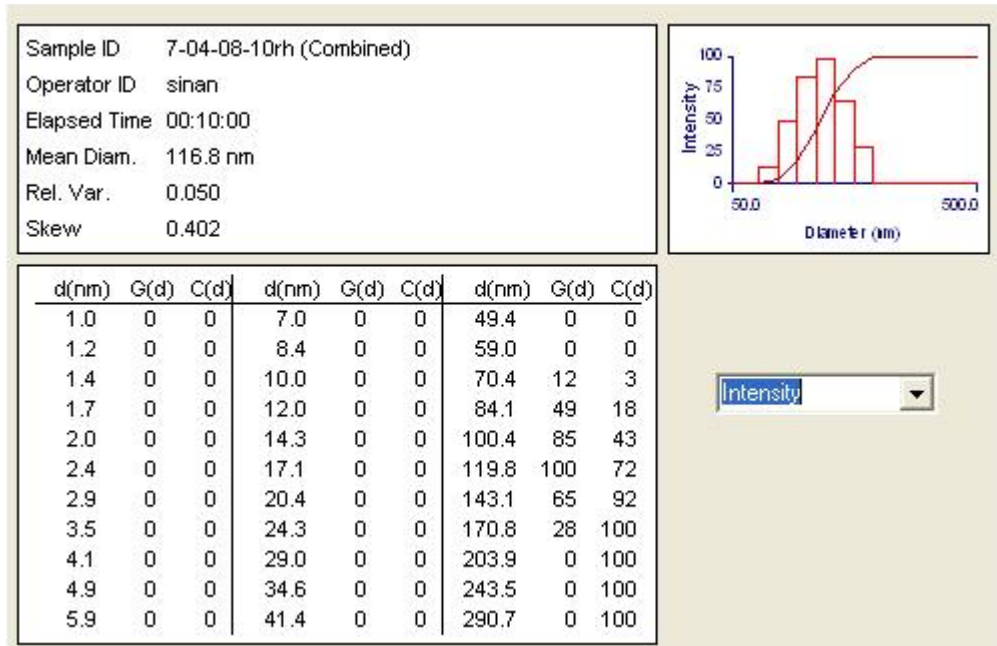
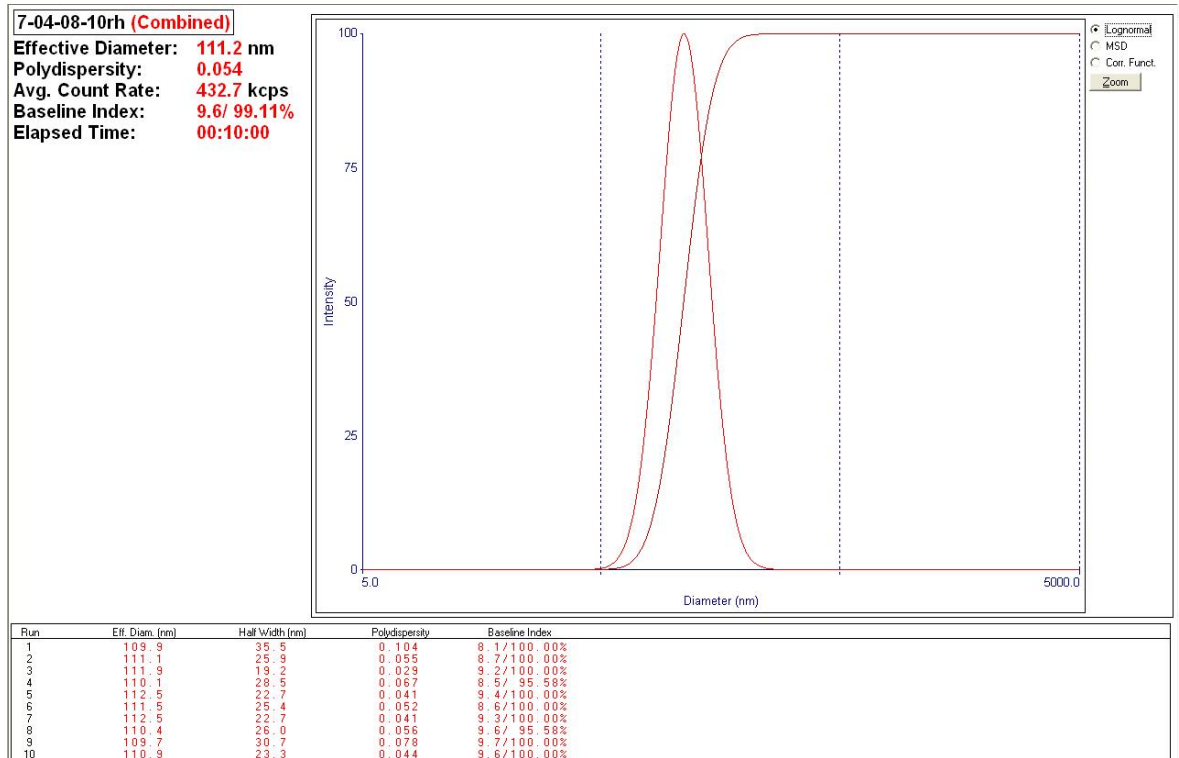
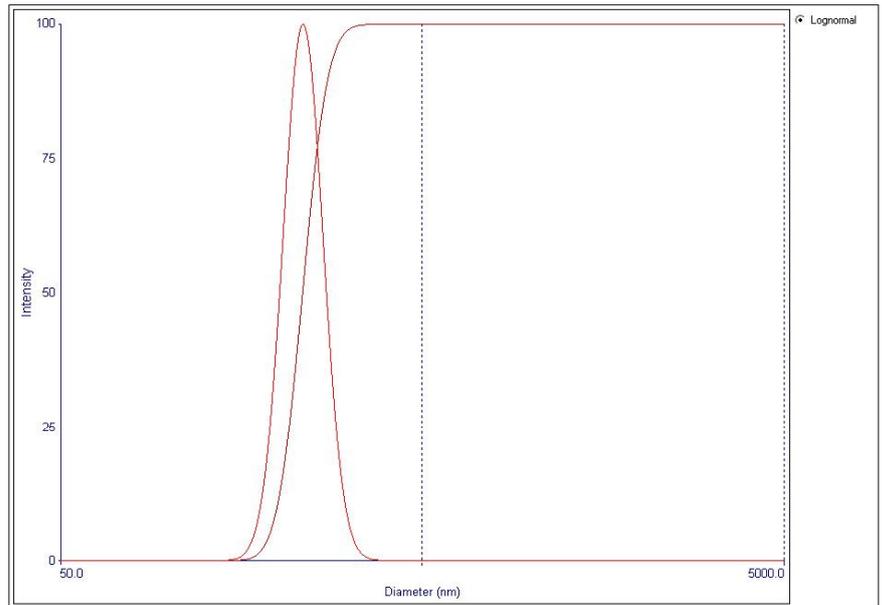


Figure A. 7. Particle size data of sample S7

08-04-08 TR (Combined)

Effective Diameter: 234.7 nm
 Polydispersity: 0.016
 Avg. Count Rate: 335.7 kcps
 Baseline Index: 8.9/ 74.37%
 Elapsed Time: 00:10:00



Run	Eff. Diam. (nm)	Half Width (nm)	Polydispersity	Baseline Index
1	233.5	27.7	0.014	7.0 / 79.67%
2	237.2	16.8	0.005	7.9 / 73.78%
3	233.2	75.4	0.105	8.0 / 58.22%
4	228.3	92.5	0.131	5.4 / 73.78%
5	240.3	52.4	0.048	1.5 / 72.44%
6	234.4	41.2	0.031	8.9 / 71.24%
7	235.0	16.9	0.005	8.0 / 66.67%
8	234.7	16.6	0.005	7.6 / 86.67%
9	231.3	37.1	0.026	9.8 / 72.89%
10	232.5	27.5	0.014	9.6 / 89.33%
Mean	234.4	39.4	0.038	7.4 / 74.37%
Std. Error	1.1	7.6	0.014	0.8 / 2.85
Combined	234.7	29.8	0.016	8.9 / 74.37%

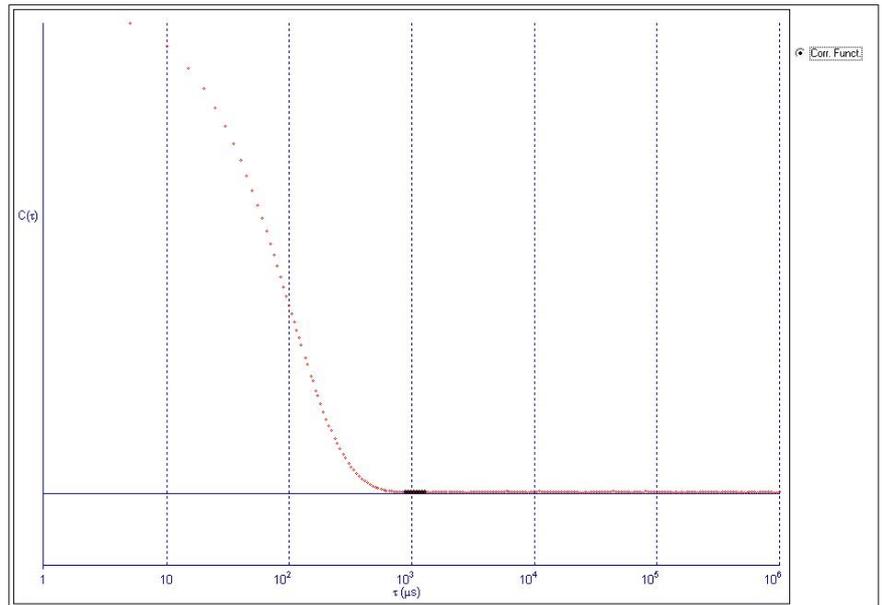
Sample ID 08-04-08 TR (Combined)
 Operator ID sinan
 Elapsed Time 00:10:00
 Mean Diam. 235.5 nm
 Rel. Var. 0.000
 Skew 0.032

d(nm)	G(d)	C(d)	d(nm)	G(d)	C(d)	d(nm)	G(d)	C(d)
227.9	0	0	233.1	0	0	238.4	0	100
228.3	0	0	233.6	0	0	238.9	0	100
228.8	0	0	234.0	0	0	239.4	0	100
229.3	0	0	234.5	31	10	239.9	0	100
229.8	0	0	235.0	66	32	240.4	0	100
230.2	0	0	235.5	100	64	240.9	0	100
230.7	0	0	236.0	71	87	241.3	0	100
231.2	0	0	236.4	36	99	241.8	0	100
231.6	0	0	236.9	2	100	242.3	0	100
232.1	0	0	237.4	0	100	242.8	0	100
232.6	0	0	237.9	0	100	243.3	0	100

Figure A. 8. Particle size data of sample S8

17-06-08-7 (Combined)

Effective Diameter: 80.4 nm
 Polydispersity: 0.065
 Avg. Count Rate: 406.1 kcps
 Baseline Index: 8.0/ 95.17%
 Elapsed Time: 00:10:00



Run	Eff. Diam. (nm)	Half Width (nm)	Polydispersity	Baseline Index
1	80.1	16.1	0.040	8.9/ 95.56%
2	79.1	21.6	0.075	7.9/ 82.22%
3	80.4	22.6	0.079	9.5/ 95.58%
4	80.7	16.8	0.043	7.6/ 95.59%
5	80.8	21.4	0.070	9.2/100.00%
6	79.5	21.7	0.074	9.7/ 91.59%
7	80.9	22.7	0.079	9.3/100.00%
8	80.3	21.5	0.072	9.0/100.00%
9	80.8	19.5	0.058	9.0/ 91.15%
10	80.1	22.1	0.076	9.2/100.00%
Mean	80.3	20.6	0.067	8.9/ 95.17%
Std. Error	0.2	0.7	0.005	0.2/ 1.80
Combined	80.4	20.5	0.065	8.0/ 95.17%

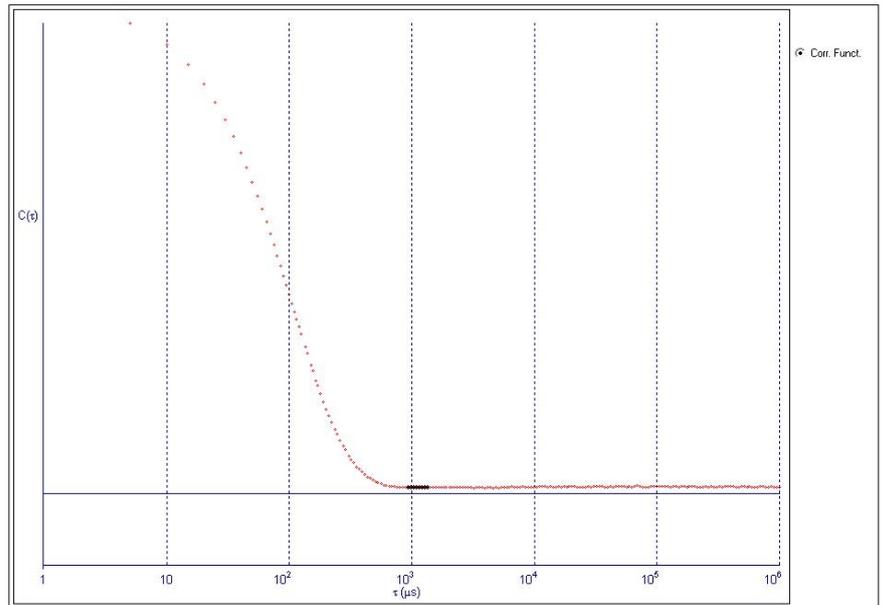
Sample ID 17-06-08-7 (Combined)
 Operator ID sinan
 Elapsed Time 00:10:00
 Mean Diam. 84.4 nm
 Rel. Var. 0.027
 Skew -3.216

d(nm)	G(d)	C(d)	d(nm)	G(d)	C(d)	d(nm)	G(d)	C(d)
18.8	0	0	36.8	0	4	71.9	0	4
20.0	0	0	39.1	0	4	76.4	33	14
21.2	0	0	41.5	0	4	81.2	70	36
22.6	4	1	44.2	0	4	86.3	100	66
24.0	5	3	46.9	0	4	91.8	71	88
25.5	4	4	49.9	0	4	97.5	35	99
27.1	0	4	53.0	0	4	103.7	4	100
28.8	0	4	56.3	0	4	110.2	0	100
30.6	0	4	59.9	0	4	117.1	0	100
32.6	0	4	63.7	0	4	124.5	0	100
34.6	0	4	67.7	0	4	132.3	0	100

Figure A. 9. Particle size data of sample S10

17-06-08-10 (Combined)

Effective Diameter: 84.2 nm
 Polydispersity: 0.059
 Avg. Count Rate: 535.2 kcps
 Baseline Index: 1.4/ 92.27%
 Elapsed Time: 00:10:00



Run	Eff. Diam. (nm)	Half Width (nm)	Polydispersity	Baseline Index
1	83.5	9.9	0.014	7.3/ 49.12%
2	84.9	22.7	0.071	9.6/ 91.15%
3	85.5	16.6	0.039	9.7/ 95.58%
4	84.2	23.0	0.074	9.2/100.00%
5	84.3	21.9	0.067	10.0/100.00%
6	82.2	23.9	0.085	10.0/ 95.58%
7	85.0	19.0	0.050	9.0/100.00%
8	83.7	19.6	0.055	9.6/100.00%
9	84.2	23.5	0.078	6.8/ 95.59%
10	84.0	19.2	0.052	8.5/ 95.59%
Mean	84.2	19.9	0.058	9.0/ 92.26%
Std. Error	0.3	1.3	0.007	0.4/ 4.88
Combined	84.2	20.4	0.059	1.4/ 92.27%

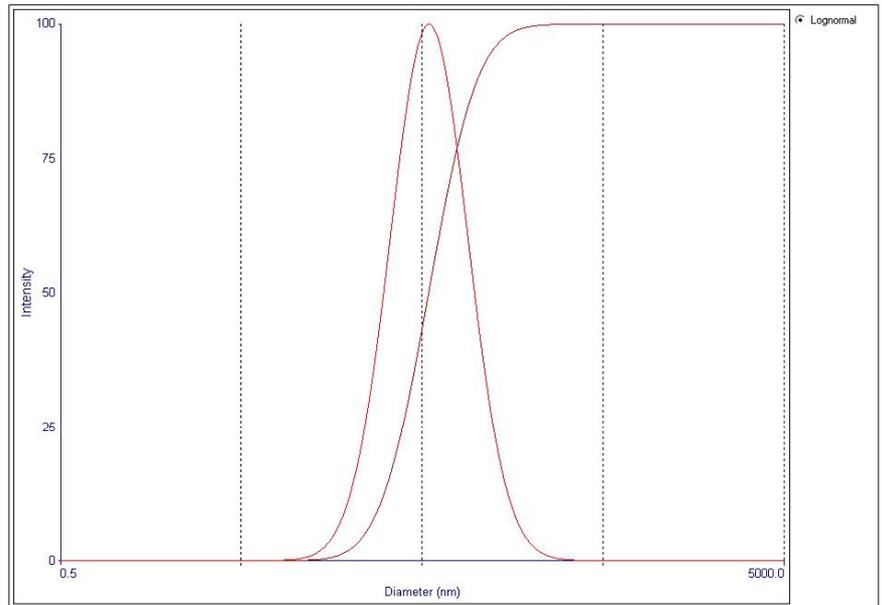
Sample ID 17-06-08-10 (Combined)
 Operator ID sinan
 Elapsed Time 00:10:00
 Mean Diam. 88.1 nm
 Rel. Var. 0.026
 Skew -3.221

d(nm)	G(d)	C(d)	d(nm)	G(d)	C(d)	d(nm)	G(d)	C(d)
24.6	0	0	42.3	0	5	72.8	0	5
25.9	0	0	44.5	0	5	76.5	0	5
27.2	3	1	46.7	0	5	80.4	19	10
28.5	4	2	49.1	0	5	84.4	62	26
30.0	5	3	51.6	0	5	88.7	100	53
31.5	3	4	54.2	0	5	93.2	100	79
33.1	3	5	56.9	0	5	97.9	58	95
34.8	0	5	59.8	0	5	102.8	20	100
36.5	0	5	62.8	0	5	108.0	0	100
38.4	0	5	66.0	0	5	113.5	0	100
40.3	0	5	69.3	0	5	119.2	0	100

Figure A. 10. Particle size data of sample S11

070708-5D (Combined)

Effective Diameter: **54.7 nm**
 Polydispersity: **0.273**
 Avg. Count Rate: **391.3 kcps**
 Baseline Index: **1.1/ 69.90%**
 Elapsed Time: **00:10:00**



Run	Eff. Diam. (nm)	Half Width (nm)	Polydispersity	Baseline Index
1	53.4	27.6	0.268	0.4/ 73.89%
2	55.2	29.0	0.275	1.2/ 65.04%
3	54.1	28.1	0.270	0.0/ 73.01%
4	54.3	28.0	0.267	0.0/ 60.62%
5	55.5	28.6	0.266	2.1/ 83.19%
6	55.0	29.9	0.285	4.7/ 69.03%
7	54.6	27.6	0.255	0.5/ 61.06%
8	54.5	27.8	0.261	0.0/ 63.27%
9	55.3	29.9	0.291	1.8/ 64.44%
10	55.2	29.3	0.282	1.9/ 85.40%
Mean	54.8	28.6	0.272	1.3/ 69.90%
Std. Error	0.2	0.3	0.004	0.5/ 2.80
Combined	54.7	28.6	0.273	1.1/ 69.90%

Sample ID 070708-5D (Combined)
 Operator ID sinan
 Elapsed Time 00:10:00
 Mean Diam. 82.0 nm
 Rel. Var. 0.347
 Skew -0.095

d(nm)	G(d)	C(d)	d(nm)	G(d)	C(d)	d(nm)	G(d)	C(d)
19.4	0	0	42.1	0	46	91.2	0	46
20.8	0	0	45.1	0	46	97.9	0	46
22.3	0	0	48.4	0	46	105.0	23	49
23.9	0	0	51.9	0	46	112.7	58	58
25.7	25	4	55.7	0	46	120.9	100	73
27.6	62	13	59.8	0	46	129.7	97	88
29.6	98	28	64.2	0	46	139.2	61	97
31.7	76	40	68.8	0	46	149.3	19	100
34.0	38	46	73.9	0	46	160.2	0	100
36.5	0	46	79.2	0	46	171.9	0	100
39.2	0	46	85.0	0	46	184.4	0	100

Figure A. 11. Particle size data of sample S13

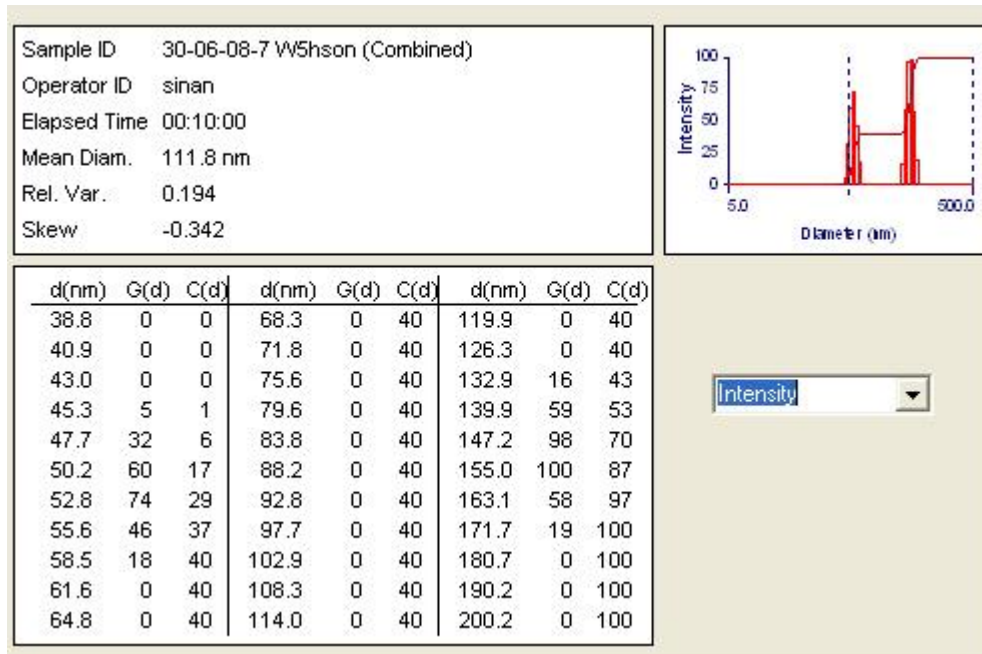
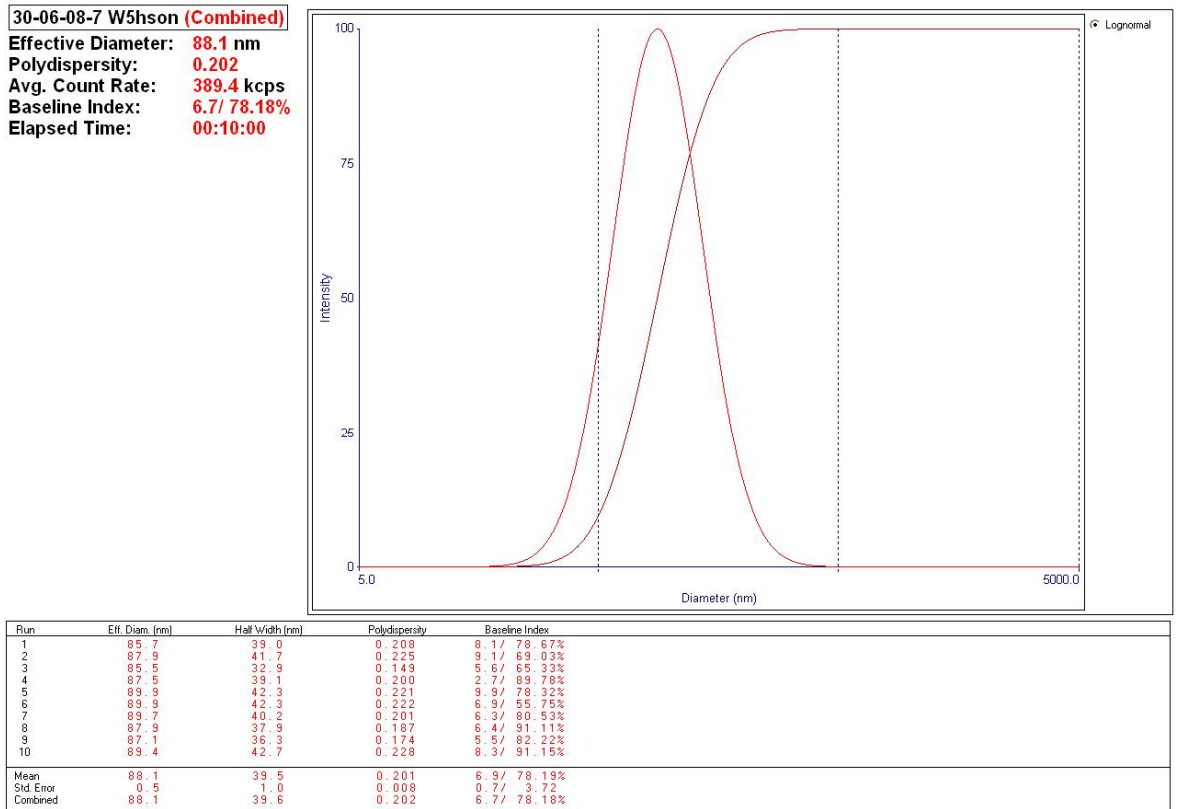


Figure A. 12. Particle size data of sample S14

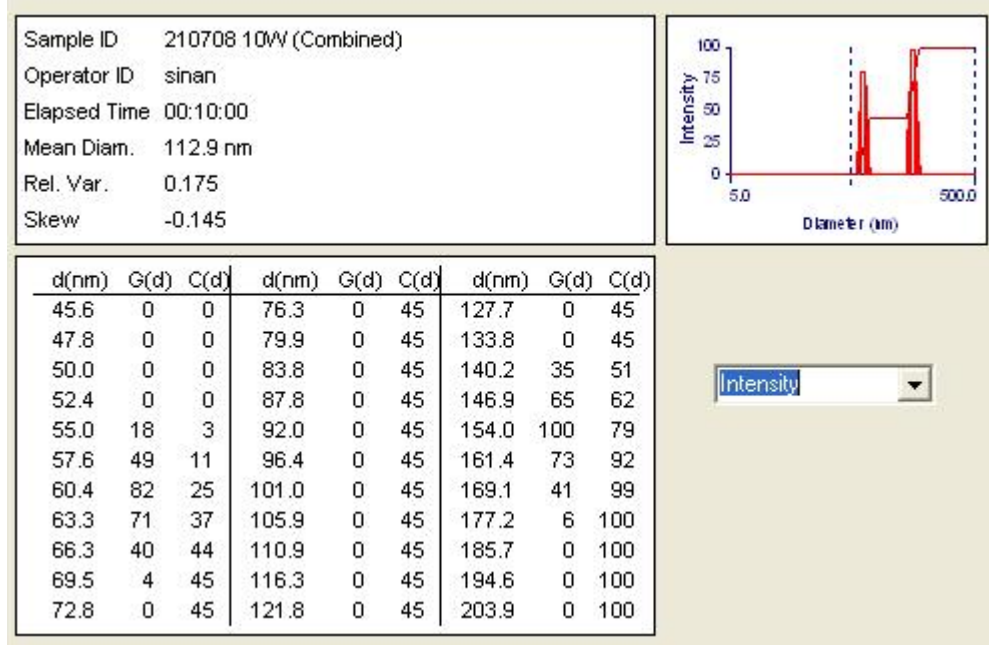
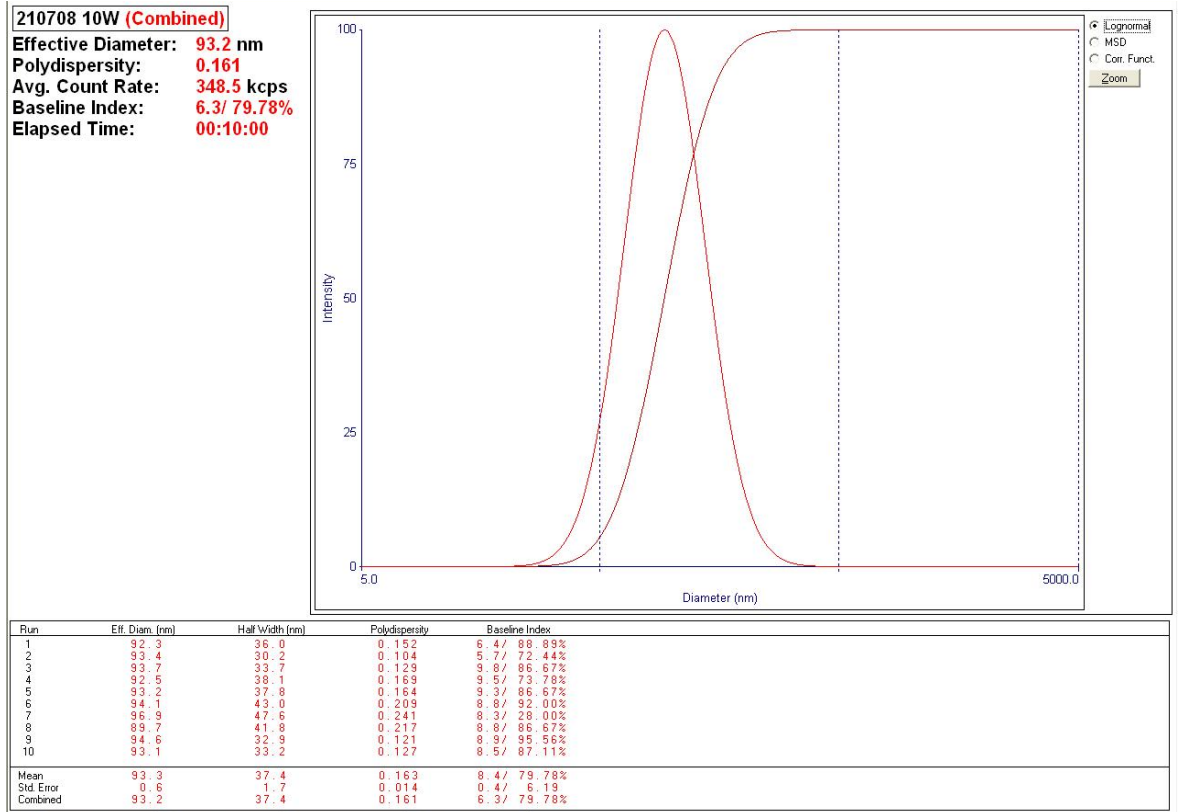


Figure A. 13. Particle size of sample S15

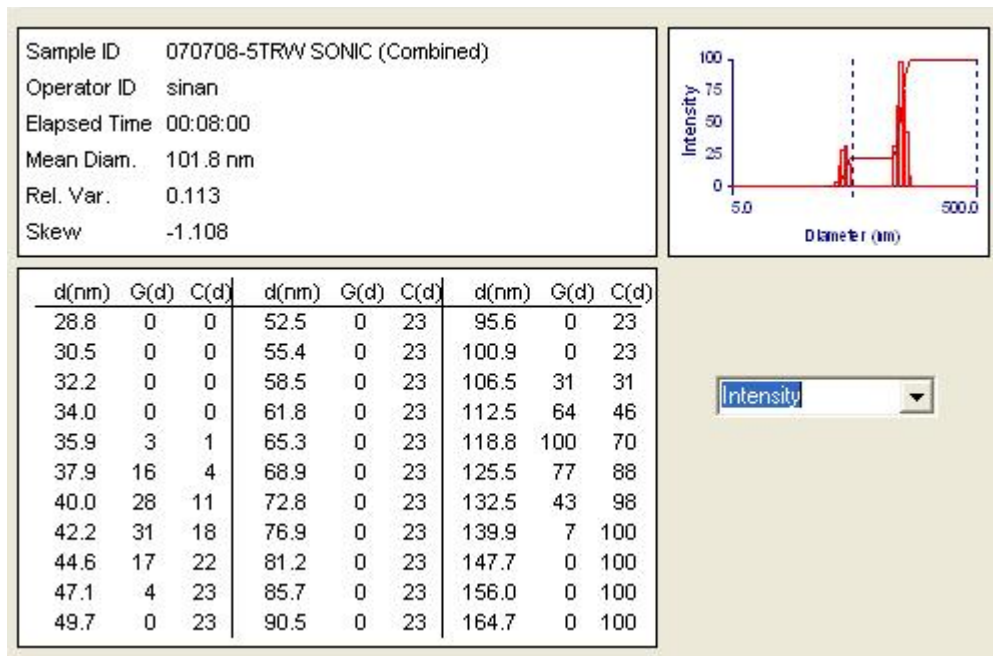
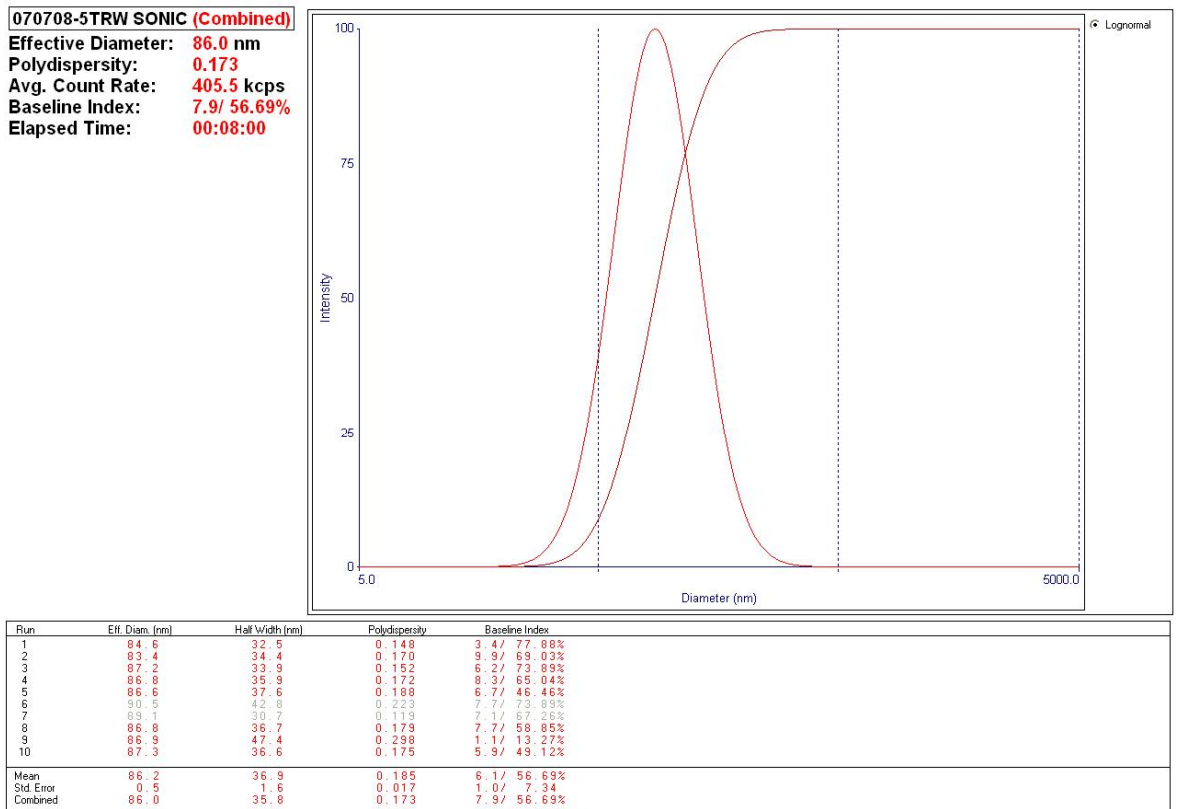


Figure A. 14. Particle size data of sample S16

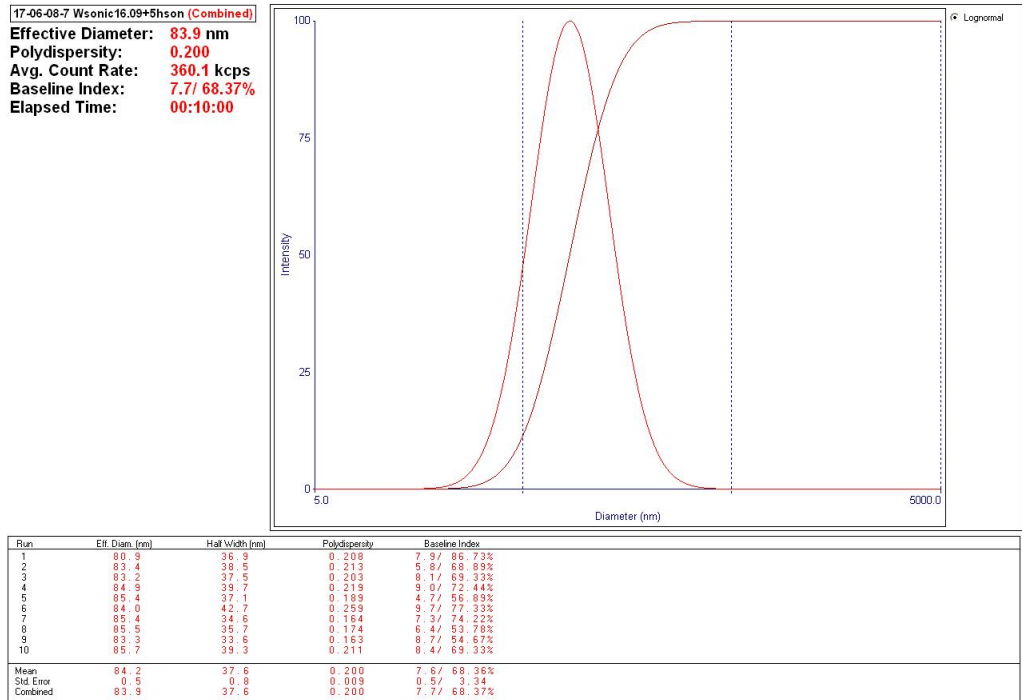


Figure A. 15. Particle size data of sample S10 in water (sonicated 5hours)

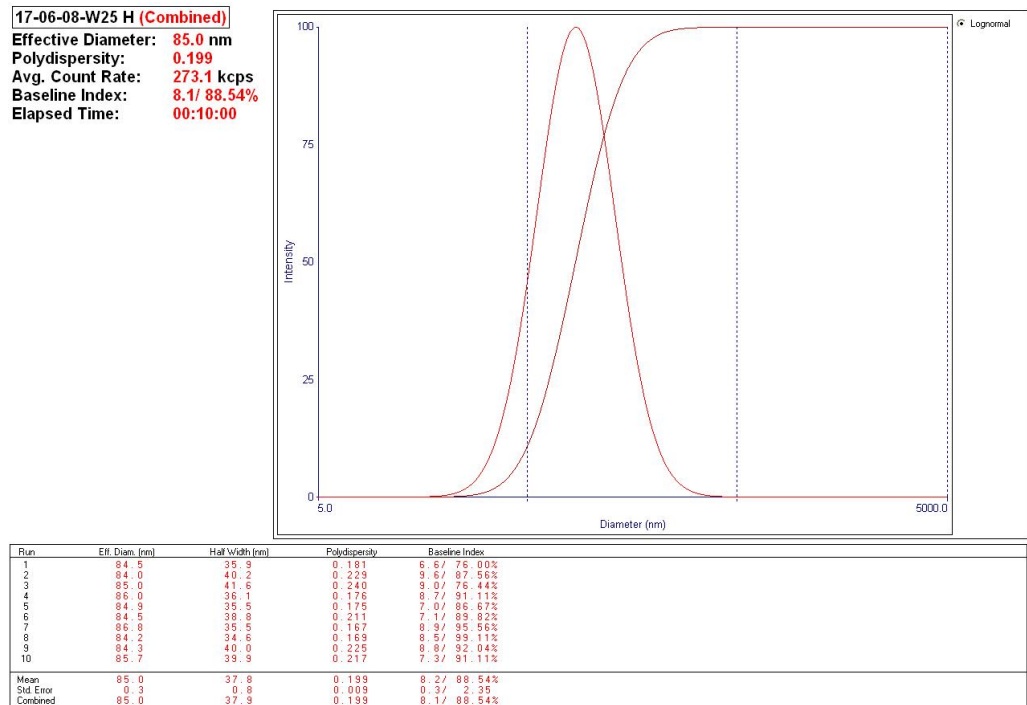


Figure A. 16. Particle size data of sample S10 in water (after 25hours)

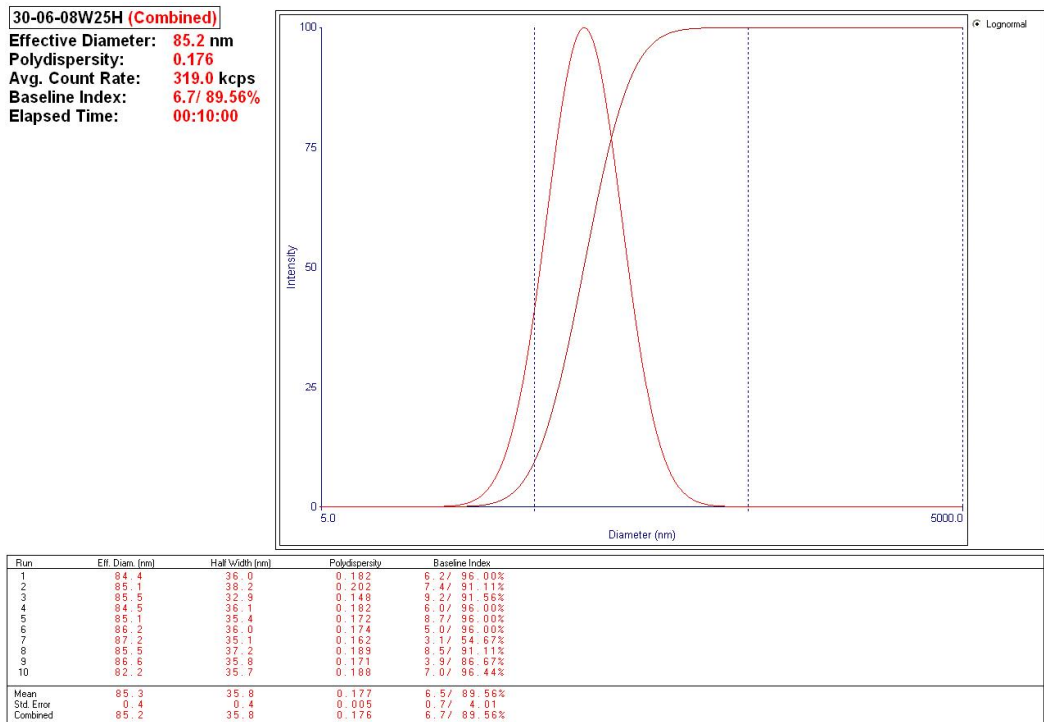


Figure A. 17. Particle size data of sample S14 in water (after 25hours)

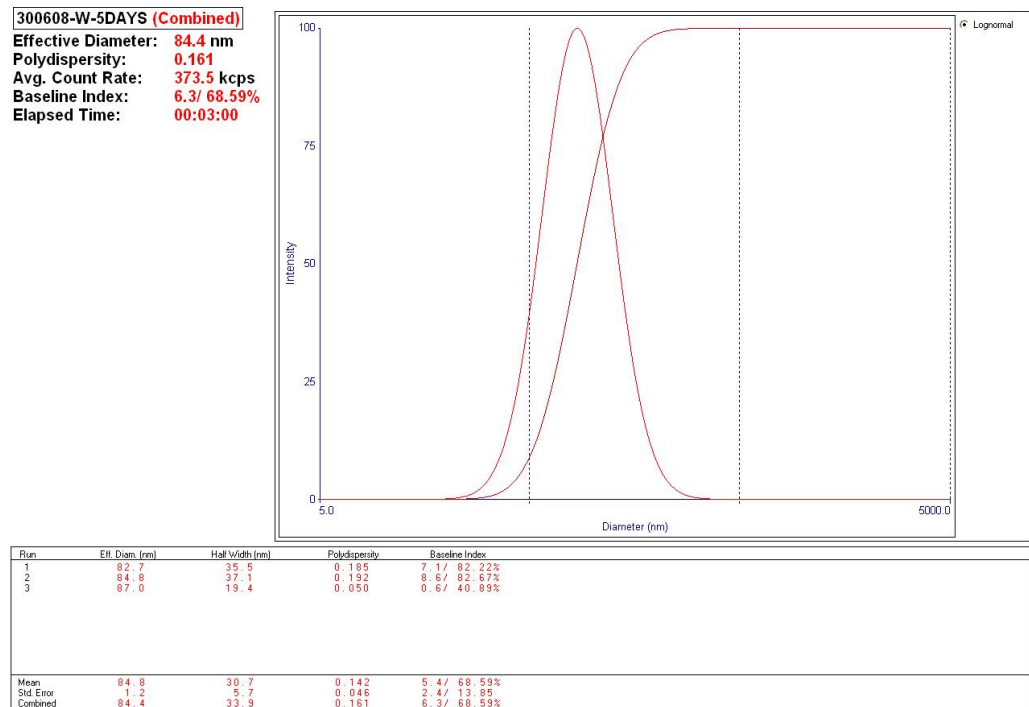


Figure A. 18. Particle size data of sample S14 in water (after 5days)

APPENDIX B: SEM RESULTS

The following pages (63-69) present the SEM results of the synthesized Silica NPs.

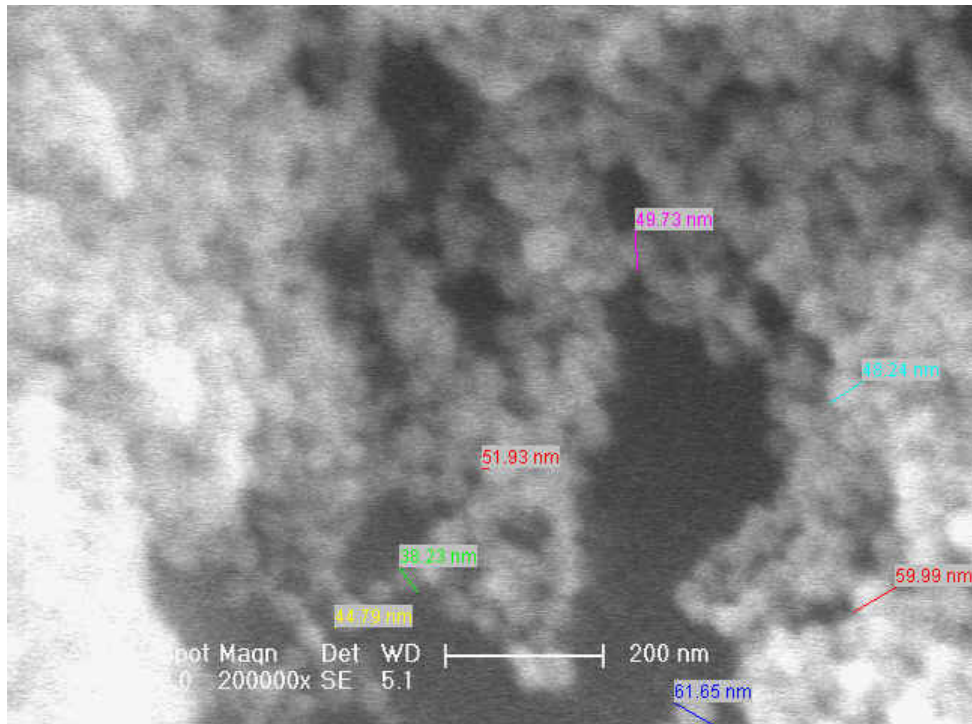


Figure B. 1. SEM image of sample S1

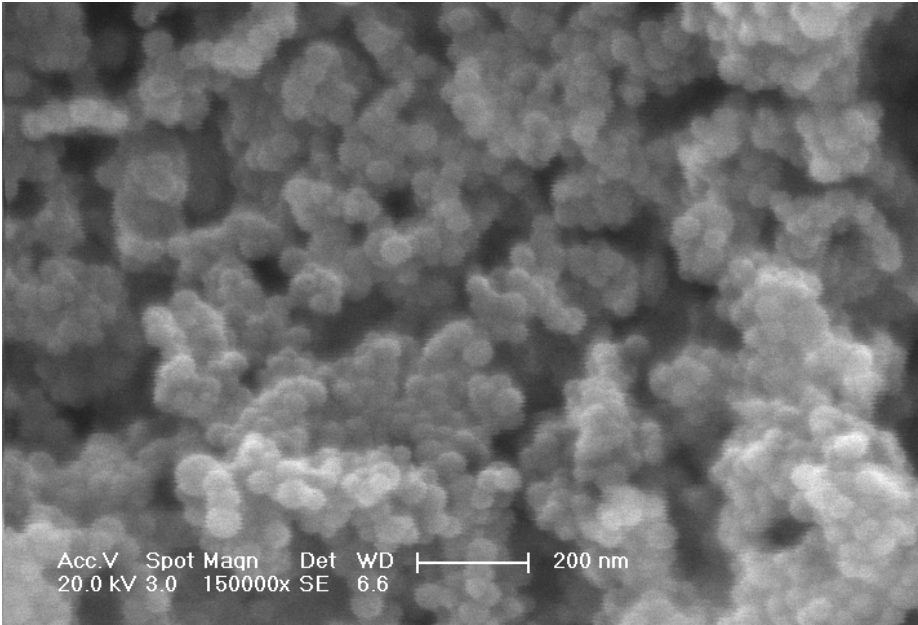


Figure B. 2. SEM image of sample S3

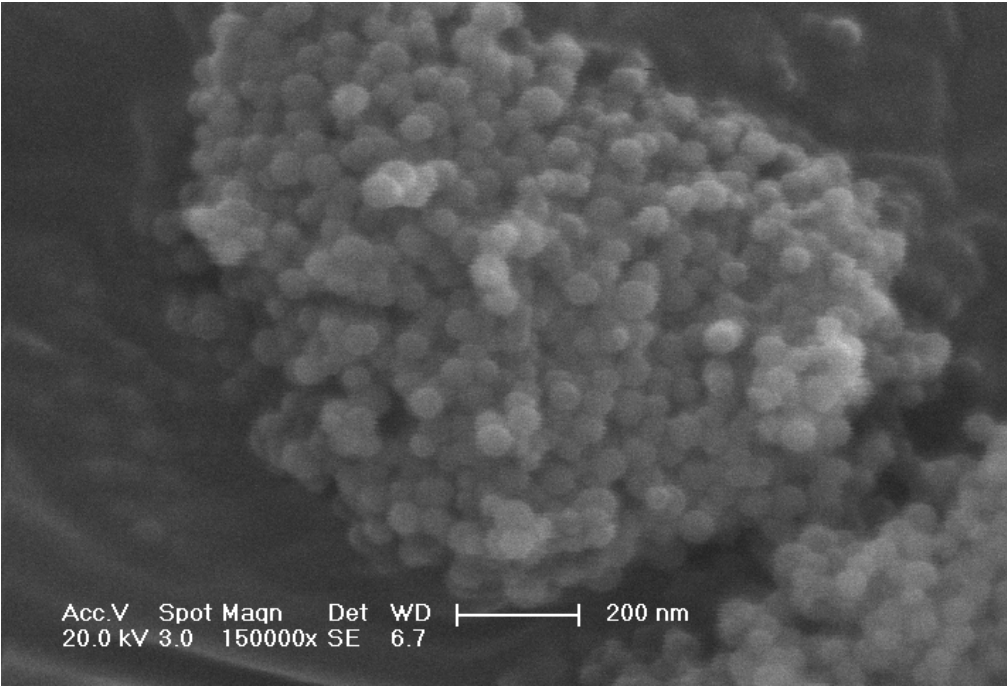


Figure B. 3. SEM image of sample S4

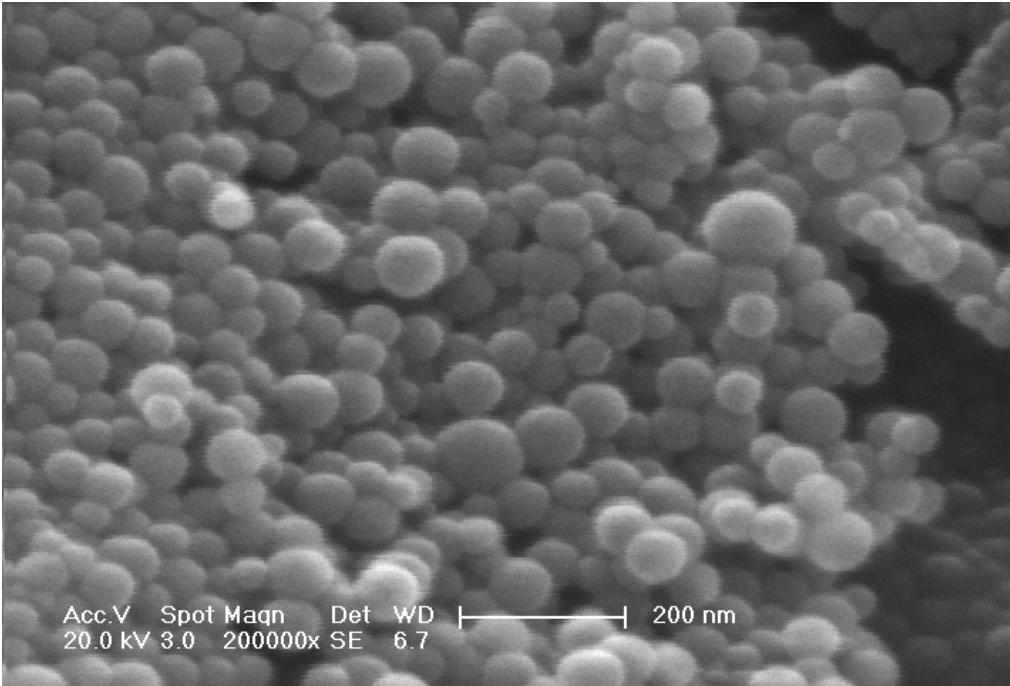


Figure B. 4. SEM image of sample S10

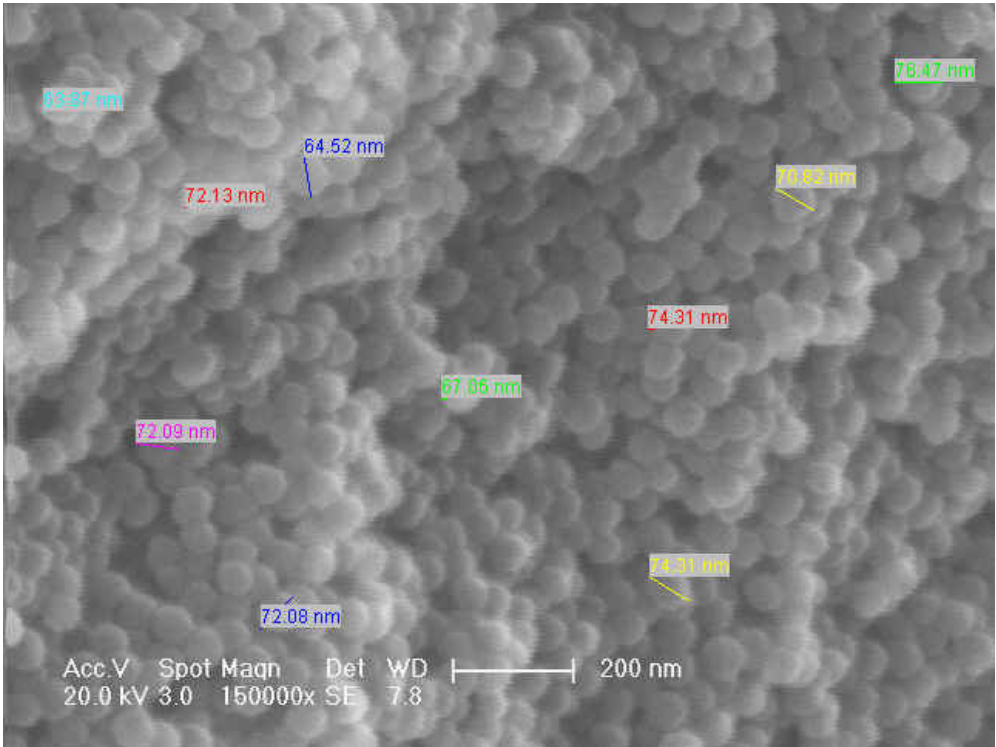


Figure B. 5. SEM image of sample S8

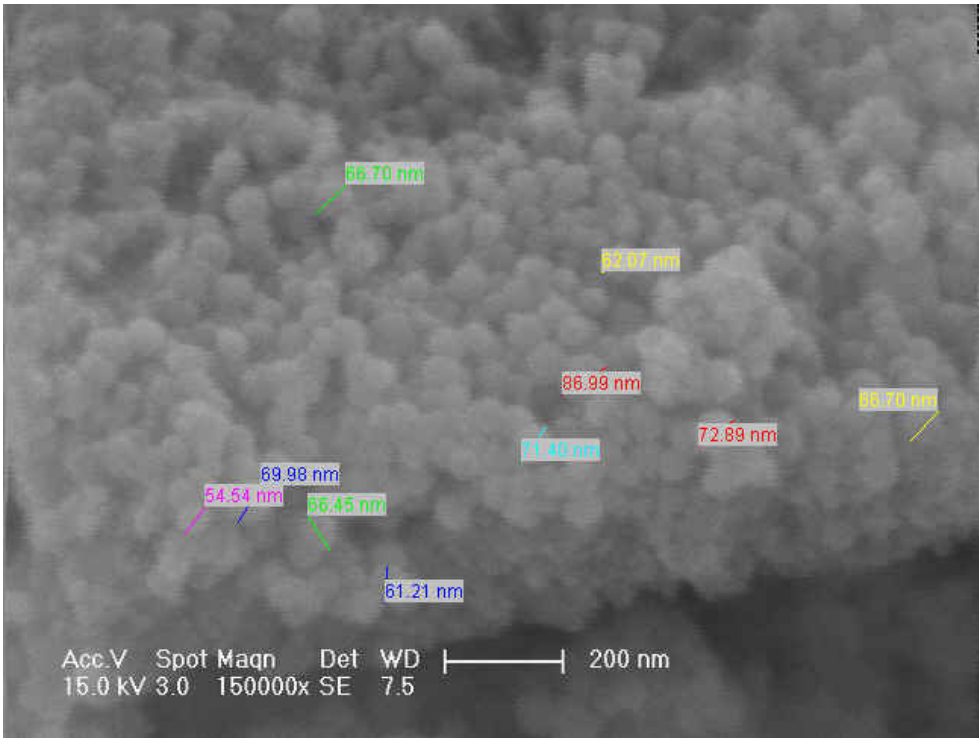


Figure B. 6. SEM image of sample S9

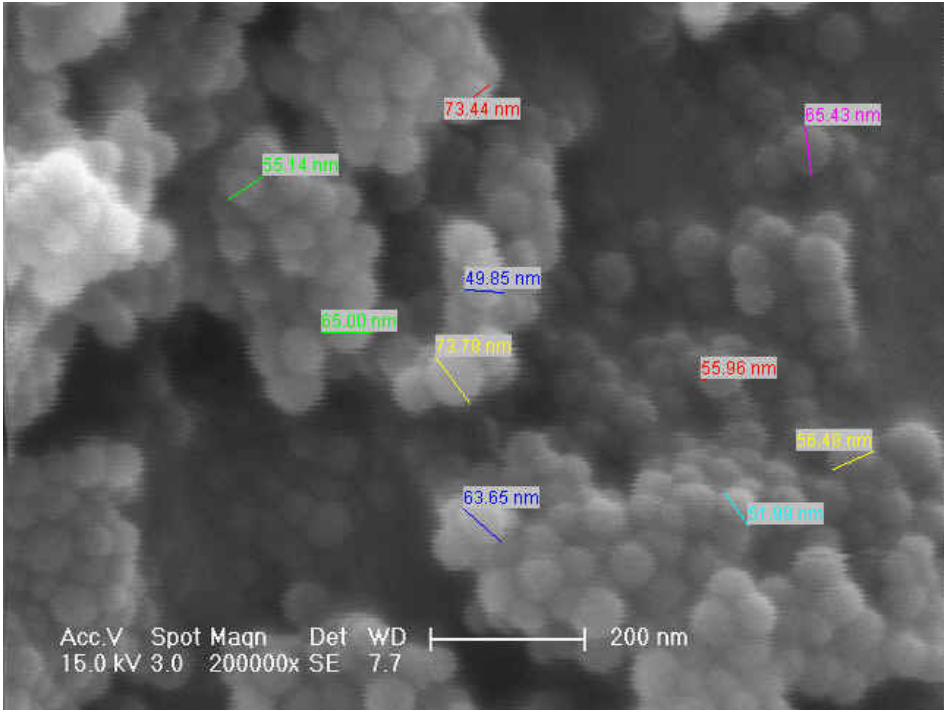


Figure B. 7. SEM image of sample S10

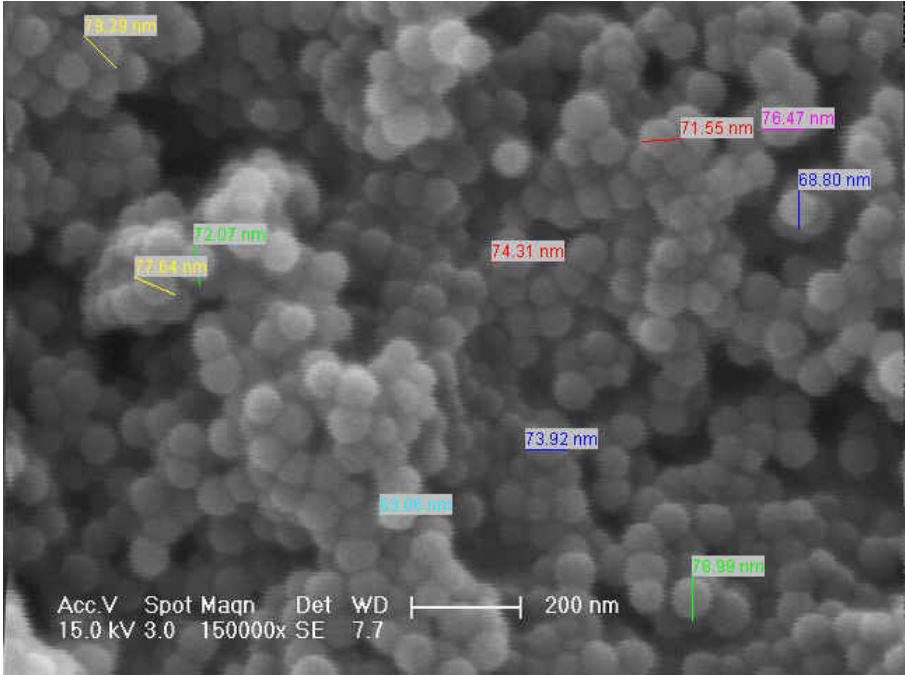


Figure B. 8. SEM image of sample S11

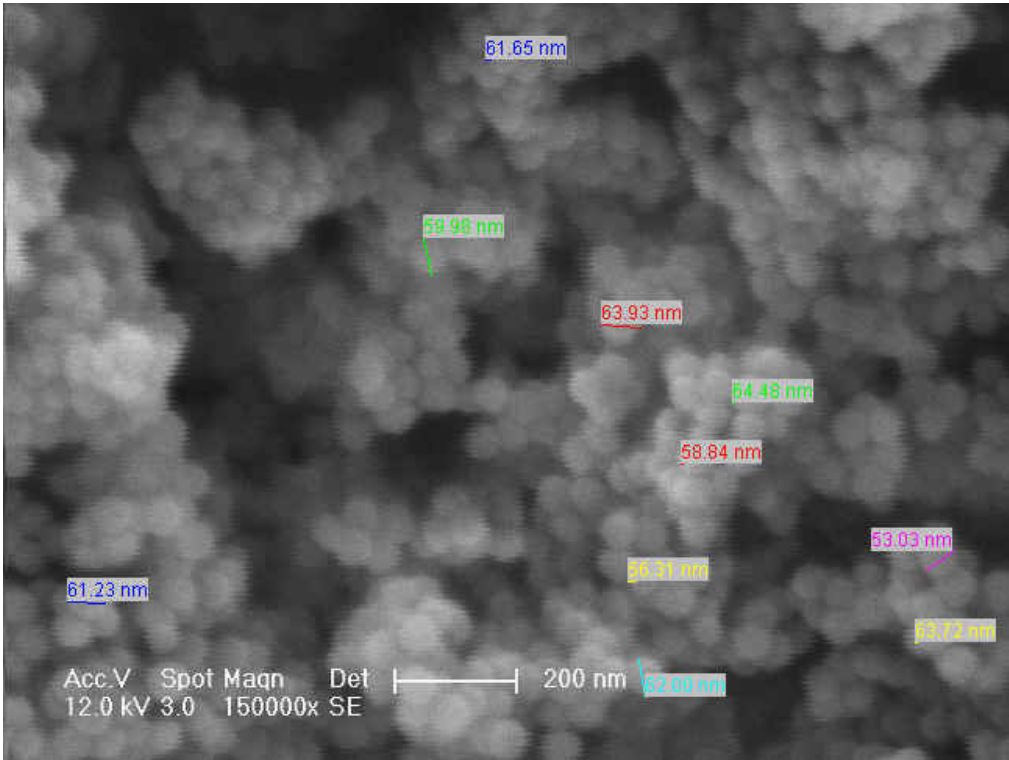


Figure B. 9. SEM image of sample S12

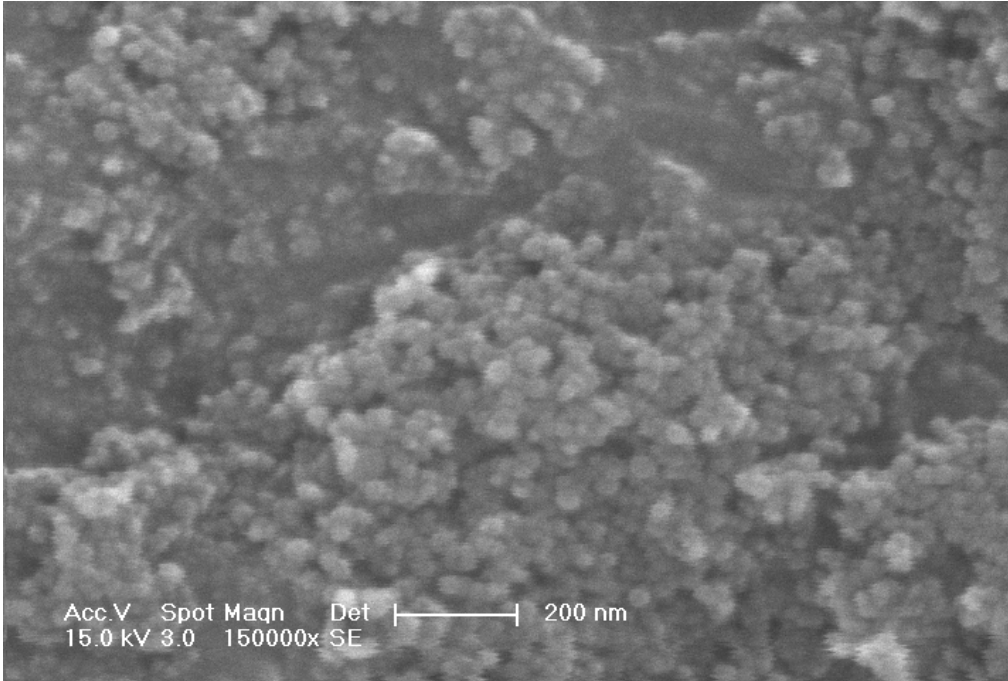


Figure B. 10. SEM image of sample S13

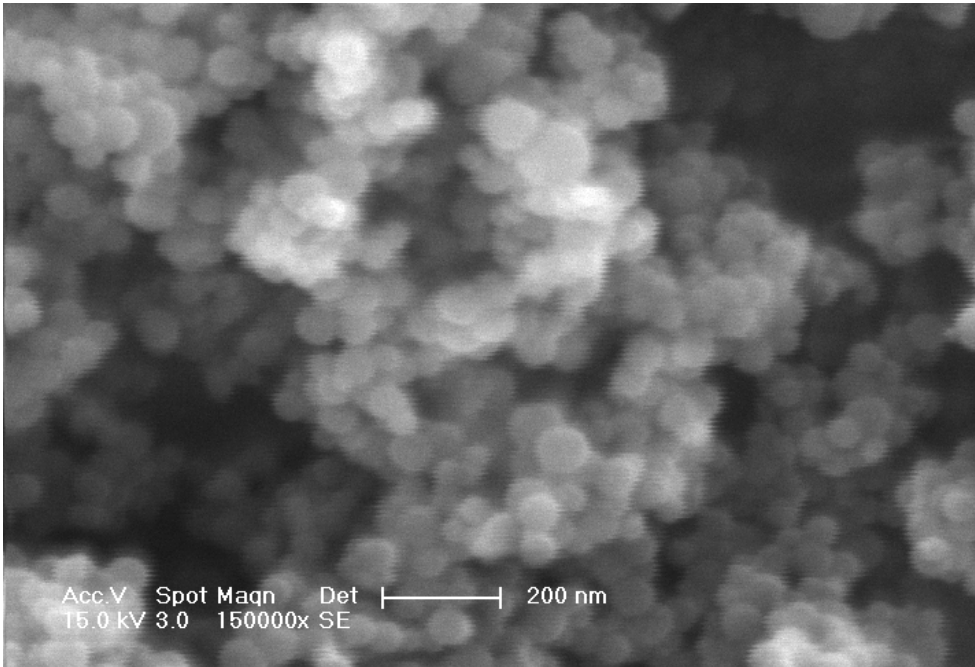


Figure B. 11. SEM image of sample S14

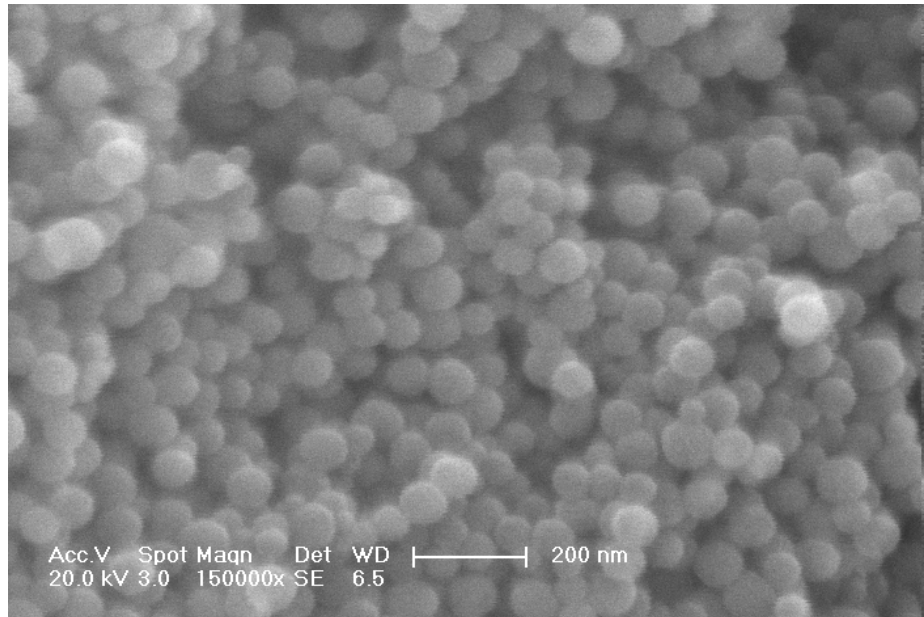


Figure B. 12. SEM image of sample S15

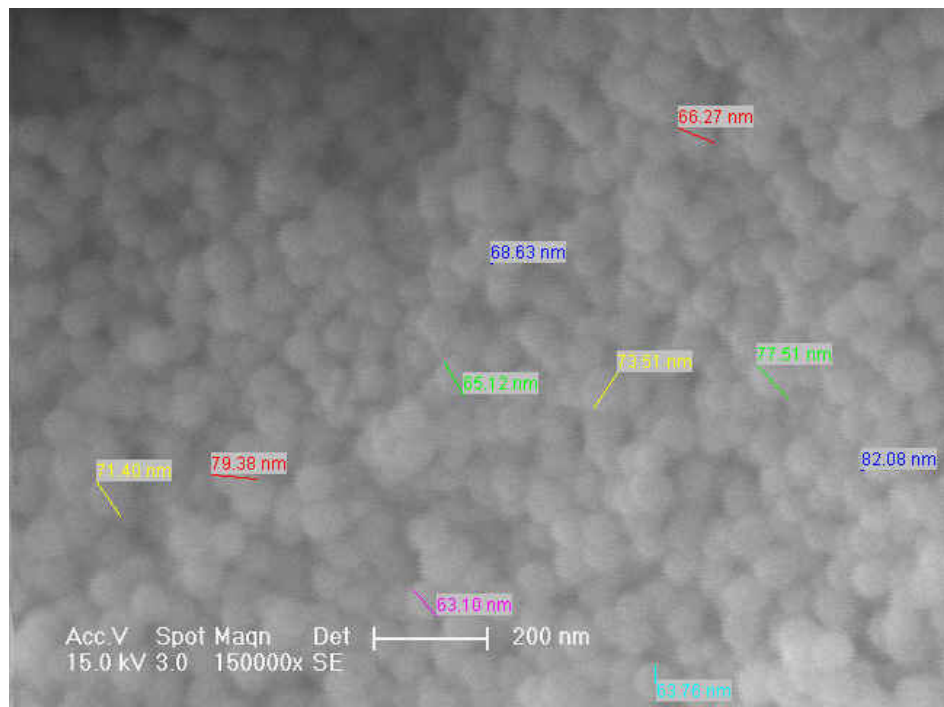


Figure B. 13. SEM image of sample S16

REFERENCES

1. Santra, S., P. Zhang, K. Wang, Tapecc, R., W. Tan, "Conjugation of biomolecules with luminophore-doped silica nanoparticles for photostable biomarkers", *Anal. Chem.*, Vol. 73, pp. 4988-4993, 2001.
2. Daniel, M. C., D. Astruc, "Gold Nanoparticles: Assembly, Supramolecular Chemistry, Quantum-Size-Related Properties, and Applications toward Biology, Catalyst, and Nanotechnology", *Chem. Rev.*, Vol. 104, pp. 293-346, 2004.
3. Nann, T., Dr. Priv-Doz, Prof. P. Mulvaney, "Single Quantum Dots in Spherical Silica Nanoparticles", *Angewandte Chemie*, Vol. 43, pp. 5393-5396, 2004.
4. Ma, Z., Y. Guan, H. Liu, "Superparamagnetic Silica Nanoparticles with Immobilized Metal Affinity Ligands for Protein Adsorption", *J. of Magnetism and Magnetic Materials*, Vol. 301, pp. 469-477, 2006.
5. Zhao, X., R.P. Bagwe, W. Tan, "Development of Organic-Dye-Doped Silica Nanoparticles in a Reverse Microemulsion", *Advanced Materials*, Vol. 16, pp. 173-176, 2004.
6. Tan, W., K. Wang, X. He, X. Zhao, T. Drake, L. Wang, R.P. Bagwe, "Bionanotechnology Based on Silica Nanoparticles", *Medicinal Research Reviews*, Vol. 24, pp. 621-638, 2004.
7. Bagwe, R.P., L.R. Hilliard, W. Tan, "Surface Modification of Silica Nanoparticles to Reduce Aggregation and Nonspecific Binding", *Langmuir*, Vol. 22, pp. 4357-4362, 2006.
8. Hilliard, L.R., X. Zhao, W. Tan, "The Immobilization of Oligonucleotides onto Silica Nanoparticles", *Anal. Chim. Acta*, Vol. 470, pp. 51-56, 2002.

9. Wang, L., G. Liu, "Templated One-step Synthesis of Compositionally Encoded Nanowire Tags", *Anal. Chem.*, Vol. 78, pp. 2461-2464, 2006.
10. Zhao, X., R. Tapeç-Dytioco, W. Tan, "Ultrasensitive DNA Detection Using Highly Fluorescent Bioconjugated Nanoparticles", *J. Am. Chem. Soc.*, Vol. 125, pp. 11474-11475, 2003.
11. Herr, J. K., J. E. Smith, C. D. Medley, D. Shangguan, W. Tan, "Aptamer Conjugated Nanoparticles for Selective Collection and Detection of Cancer", *Anal. Chem.*, Vol. 78, pp. 2918-2924, 2006.
12. Santra, S., R. Tapeç, N. Theodoropoulou, J. Dobson, A. Hebard, W. Tan, "Synthesis and Characterization of Silica Coated Iron Oxide Nanoparticles in Microemulsion: The Effect of Nonionic Surfactants", *Langmuir*, Vol. 17, pp. 2900-2903, 2001.
13. Yan, J., M. C. Estevez, J. E. Smith, K. Wang, X. He, L. Wang, W. Tan, "Dye-Doped Nanoparticles for Bioanalysis", *Nanotoday*, Vol. 2, pp. 44-50, 2007.
14. Zhao, X., L. Hilliard, S. Mechery, Y. Wang, R. Bagwe, S. Jin, W. Tan, "A Rapid Bioassay for Single Bacterial Cell Quantitation Using Bioconjugated Nanoparticles", *Proceedings of National Academy of Sciences*, Vol. 101, pp. 15027-32, 2004.
15. Ossea-Assare, K., F. J. Arrigada, "Preparation of SiO₂ Nanoparticles in a Non-ionic Reverse Micellar System", *Colloids and Surfaces*, Vol. 50, pp. 321-339, 1990.
16. Yamauchi, H., T. Ishikawa, S. Kondo, "Surface Characterization of Ultramicro Spherical Particles of Silica Prepared by w/o Microemulsion Method", *Colloids and Surfaces*, Vol. 37, pp. 71-80, 1989.

17. Bagwe, R. P., K. C. Khilar, "Effects of the Intermicellar Exchange Rate and Cations on the Size of Silver Chloride Nanoparticles Formed in Reverse Micelles of AOT", *Langmuir*, Vol. 13, pp. 6432-6438, 1997.
18. Stoeber, W., A. Fink, E. Bohn, "Controlled Growth of Monodisperse Silica Spheres in the Micron Size Range", *Journal of Colloid and Interface Science*, Vol. 26, pp. 62-69, 1968
19. Rossi, L. M., L. Shi, F. H. Quina, Z. Rosenzweig, "Stoeber Synthesis of Monodispersed Luminescent Silica Nanoparticles for Bioanalytical Assays", *Langmuir*, Vol. 21, pp. 4277-4280, 2005.
20. Eltuğral, N., 2006, Modelling of Drug Encapsulation Using Vesicles, MS Thesis, Boğaziçi University.
21. Nicholson, J. D. and F. J. Clarke, "Surfactants in Solution", in K. L. Mittal and B. Lindman (eds.), Vol. 3, pp. 1671, Plenum Press, 1984
22. Ossea-Assare, K., F. J. Arrigada, "Growth Kinetics of Nanosized Silica in a Nonionic Water-in-Oil Microemulsion: A Reverse Micellar Pseudophase Reaction Model", *Journal of Colloid and Interface Science*, Vol. 218, pp. 68-76, 1999.
23. Ossea-Assare, K., F. J. Arrigada, "Synthesis of Nanosize Silica in Aerosol OT Reverse Microemulsions", *Journal of Colloid and Interface Science*, Vol. 170, pp. 8-17, 1995.
24. Ossea-Assare, K., F. J. Arrigada, "Synthesis of Nanosize Silica in a Nonionic Water-in-Oil Microemulsion: Effects of the Water/Surfactant Molar Ratio and Ammonia Concentration", *Journal of Colloid and Interface Science*, Vol. 211, pp. 210-220, 1999.

25. Ossea-Assare, K., F. J. Arrigada, "Controlled Hydrolysis of Tetraethoxysilane in a Nonionic Water-in-Oil Microemulsion: A Statistical Model of Silica Nucleation", *Colloids and Surfaces*, Vol. 154, pp. 311-326, 1999.
26. Chang, C. L., H. S. Fogler, "Kinetics of Silica Particle Formation in Nonionic w/o Microemulsions from TEOS", *AIChE Journal*, Vol. 42, pp. 3153-3163, 1996.
27. Yao, G., L. Wang, J. Smith, J. Xu, W. Zhao, E. Lee, W. Tan, "Flodots: Luminescent Nanoparticles", *Anal. Bioanal. Chem.*, Vol. 385, pp. 518-524, 2006.
28. http://en.wikipedia.org/wiki/Transmission_electron_microscope
29. Bagwe, R. P., L. R. Hilliard, W. Tan, "Surface Modification of Silica Nanoparticles to Reduce Aggregation and Nonspecific Binding", *Langmuir*, Vol. 22, pp. 4357-4362, 2006.
30. Nagamoto, K., *Infrared and Raman Spectra of Inorganic and Coordination Compounds*, pp. 471, New York: Wiley, 1997.
31. Roy, I., Y. T. Ohulchanskyy, D. J. Bharali, H. E. Pudavar, R. A. Mistretta, N. Kaur, "Optical Tracking of Organically Modified Silica Nanoparticles as DNA Carriers: A Nonviral, Nanomedicine Approach for Gene Delivery", *PNAS*, Vol. 102, pp. 279-284, 2005.